DELIVERABLE D3.9
HYDRO-THERMAL MODEL USING VSP ANALYSIS AND COLDER REINJECTION TESTS

WP3: Upscaling of thermal power production and optimized operation of EGS plants

Contractual delivery date:	M41
Actual delivery date:	M41

PROJECT INFORMATION

Grant Agreement n°	792037
Dates	1st May 2018 – 31 October 2021

This project has received funding from the European Union's Horizon 2020 research and innovation programme under grant agreement No 792037

DOCUMENT INFORMATION

Version	VF	**Dissemination level**	PU
Editor	BAUJARD (ESG)		
Other authors	DALMAIS (ESG), ABDELFETTAH (GIMLABS), BARNES (GIMLABS), SINGH (TUDa), MAHMOODPOUR (TUDa)		

DOCUMENT APPROVAL

Name	Position in project	Organisation	Date	Visa
ALBERT GENTER	Project Coordinator	ES GEOTHERMIE	24/09/2021	OK
ELEONORE DALMAIS	WP Leader	ES GEOTHERMIE	24/09/2021	OK
JEAN HERISSON	Project Manager Officer	AYMING	23/09/2021	OK
SINGH MAHMOODPOUR	Internal reviewer	TUDa	22/09/2021	OK

DOCUMENT HISTORY

Version	Date	Modifications	Authors
V1	01/09/2021	Creation of the first version	BAUJARD, DALMAIS, ABDELFETTAH, BARNES, SINGH, MAHMOODPOUR
VF	23/09/2021	Final checks	HERISSON

CONTENT

LIST OF FIGURES

PUBLIC SUMMARY

This report describes the works related to colder fluid reinjection realised in the framework of the WP3 entitled "*Upscaling of thermal power production and optimized operation of EGS plants"*, in order to produce more energy with the same infrastructure. It is focussed on the Soultz-sous-Forêts geothermal site (France).

The works carried out are based on new and vintage geophysical data processing, analysis and interpretation (VSP and 3D seismic), analysis of 3 years operation data (flowrate, wellhead pressures, production and injection temperatures), and extensive modelling works based on well data, geophysical data and operation data, leading to detailed structural models and accurate calibrations.

It concludes that cold water reinjection might lead to a limited production temperature decrease in the particular case of Soultz-sous-Forêts, and thus validate this possibility.

1 EXECUTIVE SUMMARY

1.1 DESCRIPTION OF THE DELIVERABLE CONTENT AND PURPOSE

As a part of the MEET project, the geothermal powerplant of Soultz-sous-Forêts (Bas-Rhin, France) is investigating the possibility of producing more energy with the same infrastructure. This research project aims at studying the potential increase of electricity production by reinjecting the geothermal fluid at lower temperature. Indeed, during the operation of the powerplant, the geothermal fluid is currently reinjected at 70°C, and the MEET project aims to test its reinjection at 40°C. This temperature drop could generate several impacts on the reservoir such as induced seismicity, scaling, and cooling.

Thus, this report describes the works related to colder fluid reinjection realised in the framework of the WP3 entitled "***Upscaling of thermal power production and optimized operation of EGS plants***". The following results are presented:

1. The learnings of the experiments and research works carried out in the framework of MEET and the resulting modifications of the Soultz reservoir, structural and well model. These lessons come from:
    a. The experiments realized in Soultz to test cold reinjections, during the ENOGIA ORC test, and their observed consequences on the reservoir and the power plant are described
    b. The VSP analysis research work carried and the 3D seismic survey processing and interpretation work
    c. The comparison of the structural hypothesis needed in the preliminary model with the new structural understanding based on VSP and 3D seismic work
2. The final hydrothermal modelling work and results obtained in the Framework of the MEET project, and the final conclusions regarding cold reinjections taking in account the learnings cited above leading to predict the impact of cold reinjections on the reservoir in terms of additional cooling of the reservoir and of the production temperature.

MEET deliverables related to this report are:

- ORC Test in Soultz: D6.13 "Performance results analysis report from the 3 second demo sites"
- VSP and 3D seismic Analysis: D3.7 "Offset-VSP imaging of 3D geometry of fractures in granite"
- HT model for colder reinjection prediction: D3.3 "Hydro-thermal model matching colder reinjection design"
- Cold fluid chemical and physical tests: D3.10 "Summary of chemical and physical tests for colder reinjection"

The purpose of this deliverable is to quantify the impact of cold fluid reinjections on the reservoir and on the production temperature, using numerical models based on reprocessed geophysical data (VSP and 3D seismic), validated on field data

(from the experimental Soultz site) with an iterative modelling approach, and to assess the uncertainty on these results.

1.2 BRIEF DESCRIPTION OF THE STATE OF THE ART AND THE INNOVATION BREAKTHROUGHS

The Soultz-sous-Forêts EGS site is probably the most investigated site worldwide in terms of geoscientific studies. More than 60 PhD thesis have been published as well as more than 300 peer review papers published within scientific journals. Concerning structural and hydrothermal modelling, a few studies have been done over the last years.

Several structural modelling works were carried out on the Soultz site prior to the MEET project. On the structural part, a first 3D model has been created by Renard et Courrioux (1994) based on 2D seismic interpretation done by BRGM (Cautru in Menjoz et al., 1988). These interpretations have been then reworked and integrated in a comprehensive 3D model by Sausse et al. (2010). Later on, Place et al. (2010) have updated the 3D structural model but mainly in the sedimentary part by reprocessing and thus reinterpreting a 2D seismic line done for oil exploration calls PHN84J.
Numerical hydro-thermal simulation works, based on hydraulic tests of the wells and tracer experiments, also lead to significant improvement of the understanding of reservoir in the past (see for example Egert et al., 2019).

Nevertheless, this MEET deliverable D3.9 presents an unprecedented work of integration of various data types:

- Geophysical data (well data, reprocessed VSP and 3D seismic) to get the most accurate structural model on which are based the numerical simulations
- Experimental data used for calibration and history matching of the models, as 3 years operation data of the 3 wells GPK-2, GPK-3 and GPK-4 were made available for the modelling teams (operating pressure, temperature and flowrate)
- Validation data of the model with varying injection temperature

It must be pointed out that hydro-thermal simulations in fractured rocks are challenging as flowpaths in these rocks show great variability.
Thus, this is the first time that such a complete dataset is combined within a data integration and modelling effort to quantify at best the impact of cold fluid reinjections in a deep fractured reservoir.

1.3 CORRECTIVE ACTION

This deliverable D3.9, initially scheduled to M38 was delayed by 3 months as the Soultz EGS plant was shut down between September 2020 and March 2021 because of an unexpected breakdown found on the production pump, which also delayed the ORC test, as mentioned in amendment n°2 to the grant agreement.

1.4 IPR ISSUES

The works carried out in the MEET tasks related to this deliverable are based on Soultz operation data (pressure, temperature) from the Soultz-sous-Forêts power plant, which belongs to the site owner GEIE EMC and needs to remain confidential. MEET partners have access to this data according to a specific agreement with GEIE EMC for the MEET project. Therefore, as this report is a public report, some operation and geophysical data are purposely hidden.

2 DELIVERABLE REPORT

2.1 GENERAL INTRODUCTION

2.1.1 Soultz-sous-Forêts geothermal site overview

The Upper Rhine Graben is known as a great potential for the exploitation of geothermal energy at high temperature. Indeed, it presents geothermal anomalies. Usually, the geothermal gradient in continental crust is about 30°C/km. For example, it can reach 100°C/km in the sedimentary units because of the presence of large convection loops in the granitic basement and the Triassic sandstone, up to the Muschelkalk in some parts of the graben (Figure 1).

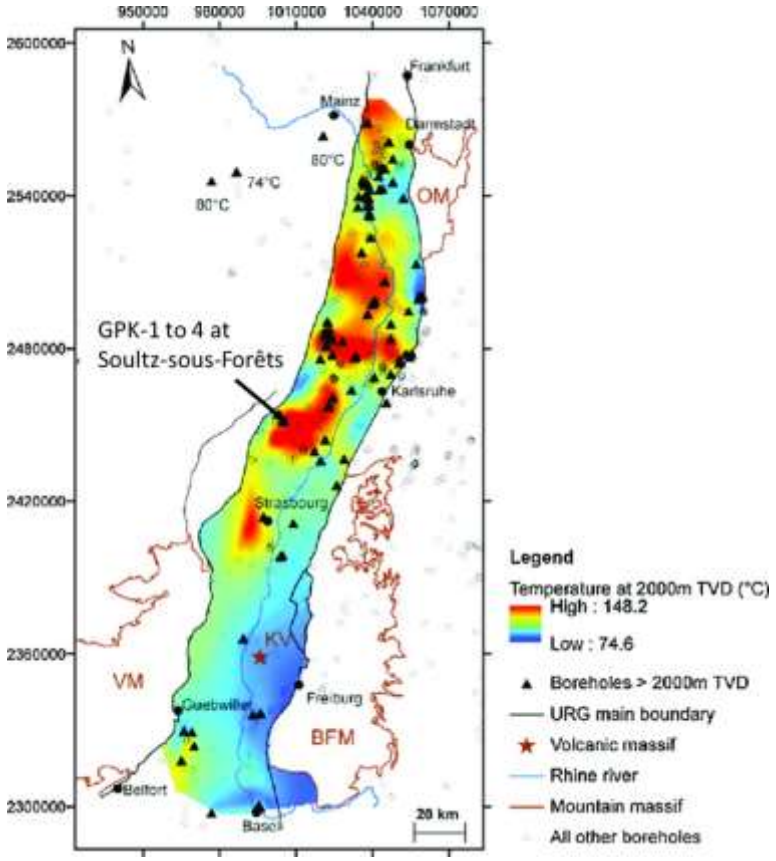

Figure 1: Temperature distribution at 2000 m TVD in the Upper Rhine Graben (modified after Baillieux et al., 2013 based on Agemar et al., 2012 and Pribnow and Schellschmidt, 2000).

Soultz-sous-Forêts is located at around 50 km north of Strasbourg in the Upper Rhine Graben (Figure 2). The geothermal project began in 1984 and first drilling began in 1987 (Gerard et al., 2006). The initial goal was to use the heat in the deep crystalline rocks to produce electricity by fracturing the granite to create an artificial reservoir as an HDR (Hot Dry Rock) project. For this, a first phase of drilling and observation was done until 2007 to study the crystalline rock and the feasibility of future operations. The geothermal fluid is a 100 g/l NaCl type brine. Hydraulic, thermal and chemical stimulations were done to

increase the permeability and the connections between the reservoir and the wells. The term of EGS (Enhanced Geothermal System) was defined from the research work of Soultz-sous-Forêts. The site gradually shifted from research to industrial facility. The industrial electricity production began in June 2016.

Three wells are currently operated: GPK-2, GPK-3 and GPK-4, reaching more than 5000 m depth. Their trajectories are distributed in a North-South direction, following main faults. GPK-2 is the production well and GPK-3 and GPK-4 are used as injection wells. The powerplant is using an ORC (Organic Rankle Cycle) to convert the heat in electricity. Indeed, the geothermal fluid is produced by GPK-2 then heats an organic fluid (isobutane) that will activate the turbine to produce electricity. During this process, the geothermal fluid is cooled down and is finally reinjected in the reservoir. Currently, the powerplant is producing a fluid at more than 150°C and the injection temperature is about 70°C.

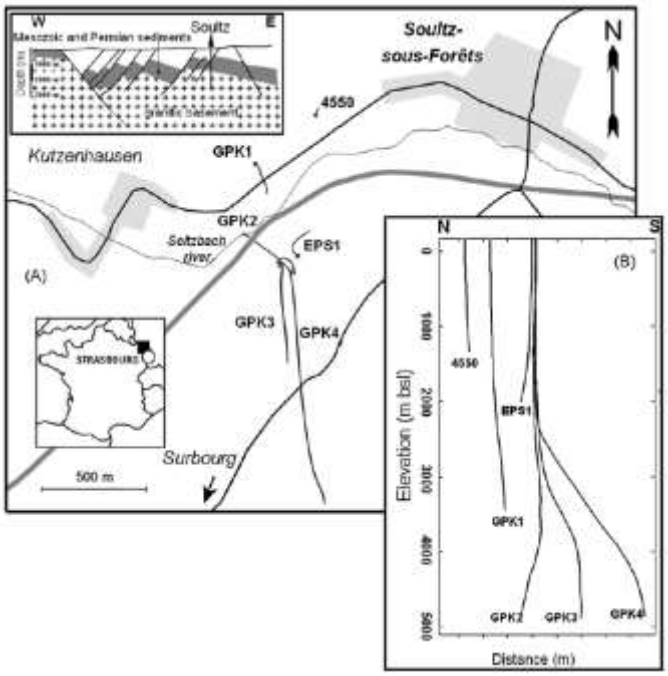

Figure 2: Location of the Soultz-sous-Forêts site, schematic geological cross-section and well paths (Sausse et al., 2010 modified after Dezayes et al, 2005).

2.1.2 Soultz-sous-Forêts wells dataset

The powerplant is operated with GPK-2 as producer and GPK-3 and GPK-4 as injectors. GPK-2, GPK-3 and GPK-4 are cemented to 1431, 1447 and 1446 m MDGL (Measured Depth from Ground Level) respectively. Under these depths, GPK-2 has been drilled in 8''1/2 until 5057 m MDGL and cased in 7'' until 4440 m MDGL. GPK-3 and GPK-4 have been drilled in 9"5/8 until 4592 and 4767 m MDGL and in 8"1/2 until 5111 and 5270 m MDGL (Figure 3). In those wells, a zone between 4000 m and 4500 m TVD is cemented. GPK-2 is cemented between 4200 m and 4500 m.

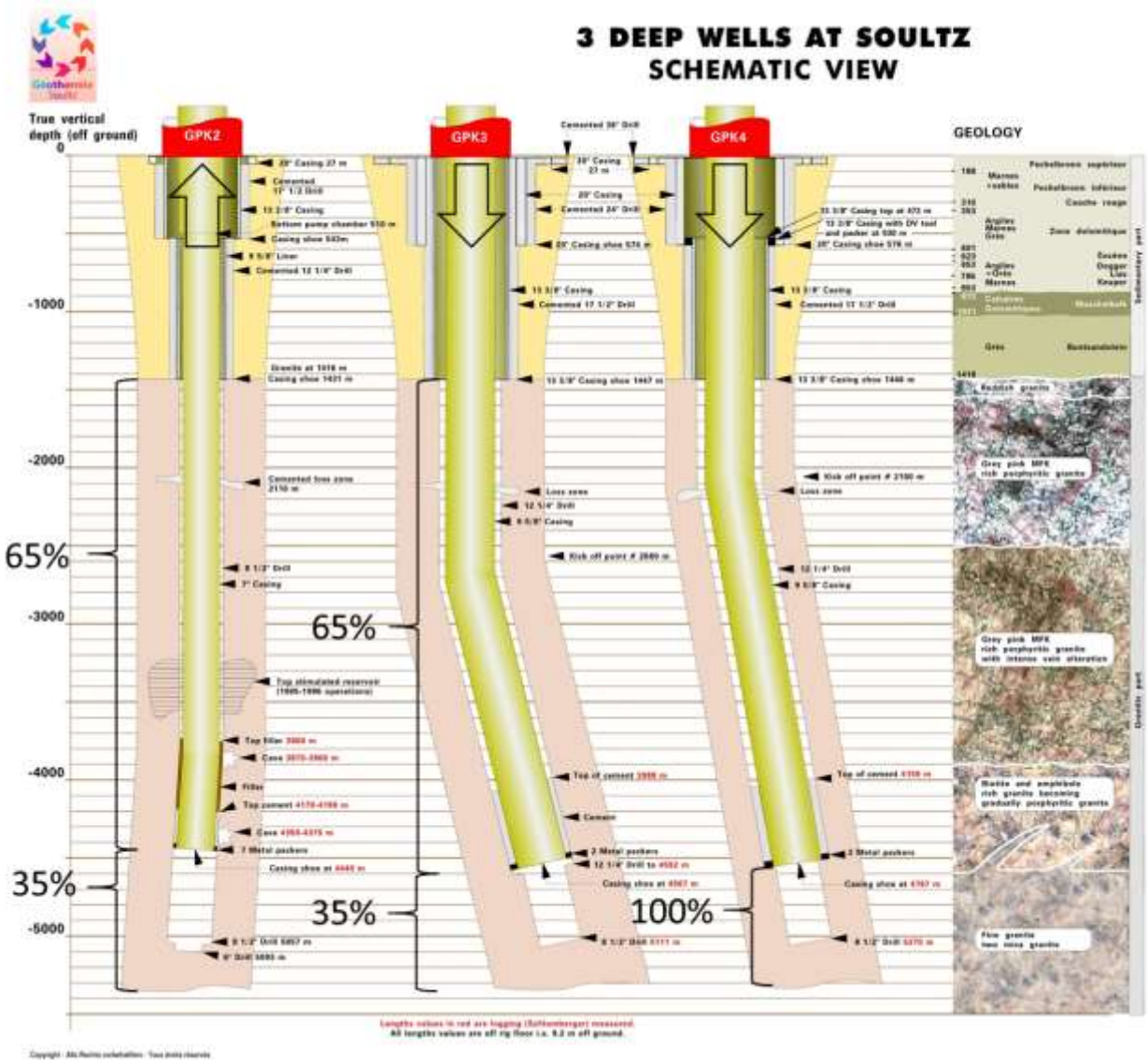

Figure 3: Completion of wells with contribution (%) of the flow. Source GEIE EMC.

Feeding zones behind the casing have been reported (Held et al., 2014) in the upper granite reservoir section of GPK-2 and GPK-3 connecting the well to its annulus from respectively 1431 and 1447 m MDGL to 4170 and 3988 m MDGL. GPK-4 doesn't present any significant leaks in its casing between 1400 m and 4500 m.

2.1.3 Soultz-sous-Forêts operation dataset

Operation data used for model calibration range from 25/06/2016 to 24/06/2019 (3 years). The average production rate is 25-30 L/s. Injection is 100% in GPK-3 until beginning of March 2017 (almost 7 months) and is then partitioned in GPK-3 and GPK-4 (Figure 4).

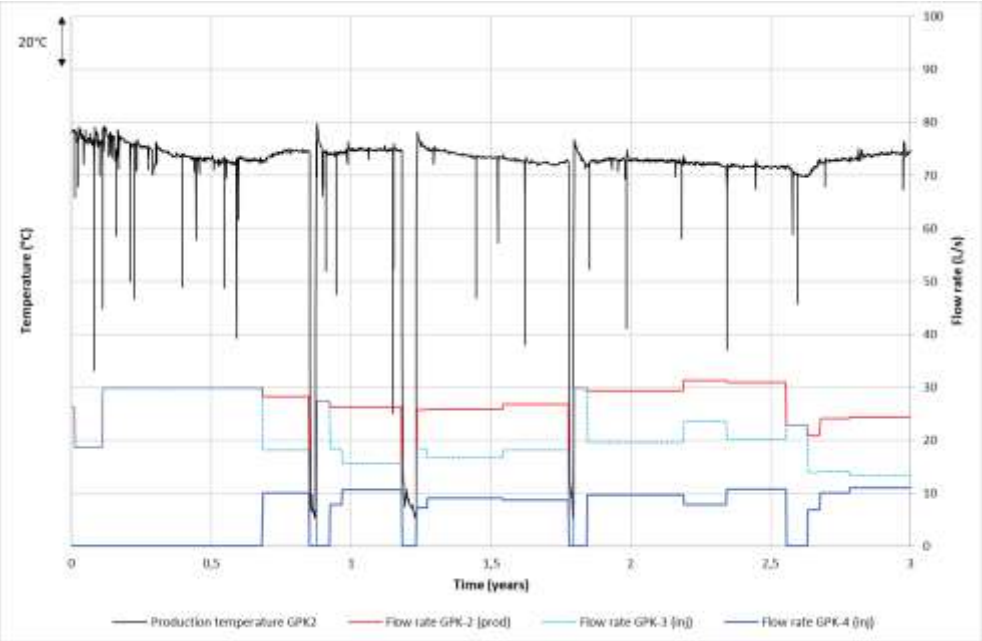

Figure 4: Soultz-sous-Forêts operation data used for model calibration. Temperature absolute values are hidden for confidentiality reasons. Source GEIE EMC.

2.2 LEARNINGS FROM EXPERIMENTS

2.2.1 Cold reinjection

2.2.1.1 ORC Test

The small-scale ORC was delivered in Soultz-sous-Forêts in August 2020. The electrical and hydraulic connection was carried out immediately. Unfortunately, the commissioning could not take place in September 2020 as planned because of a problem of the on the production pump installed in production well GPK-2. The pump had to be pulled out and sent back to manufacturer in US. The plant could be started again by the end of February 2021. The MEET ORC was operating from March 13th, 2021 until June 15th, 2021 (see Figure 5), for a total operation time of 3 months.

Figure 5: First granitic demonstration site with ORC connected to the Soultz-sous-Forêts geothermal process.

On preliminary results of the ORC tests, it can be seen that the ORC module has a stable production around 16 kW. Production is highly dependent on ambient temperature, the lower the ambient temperature the better the production (Figure 6).

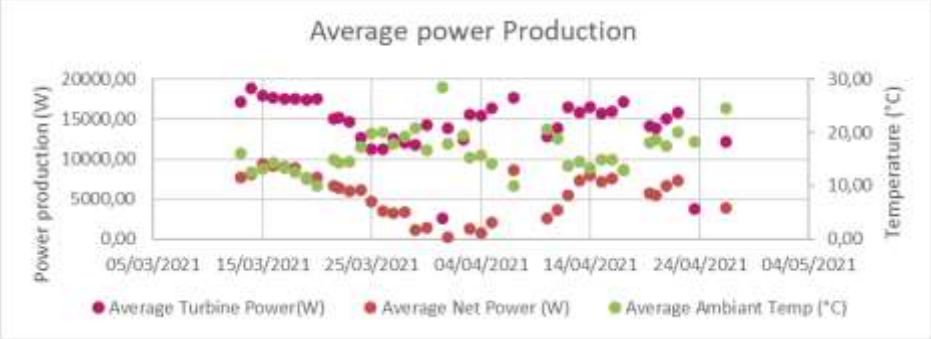

Figure 6: Plot of the average power production, and ambient temperature on the Soultz-sous- Forêts demonstration site (these preliminary results do not show the entire testing sequence).

Even if the ambient temperature during the test was not very warm for the period in this region (average temperature below 10°C), it turns out that the ORC use had no impact on reinjection temperature (see Figure 7). Reinjection temperature is mainly controlled by the main power plant ORC efficiency, which is dependent on outdoor temperature, and it seems that the additional ORC power (16 kW mean power) is too low in comparison of the main ORC (installed power 1700 kW) to produce a significant temperature change of reinjection temperature.
As the fluid is kept under pressure in the geothermal loop in order to avoid CO_2 degassing it was not possible to influence the reinjection temperature by artificial means.

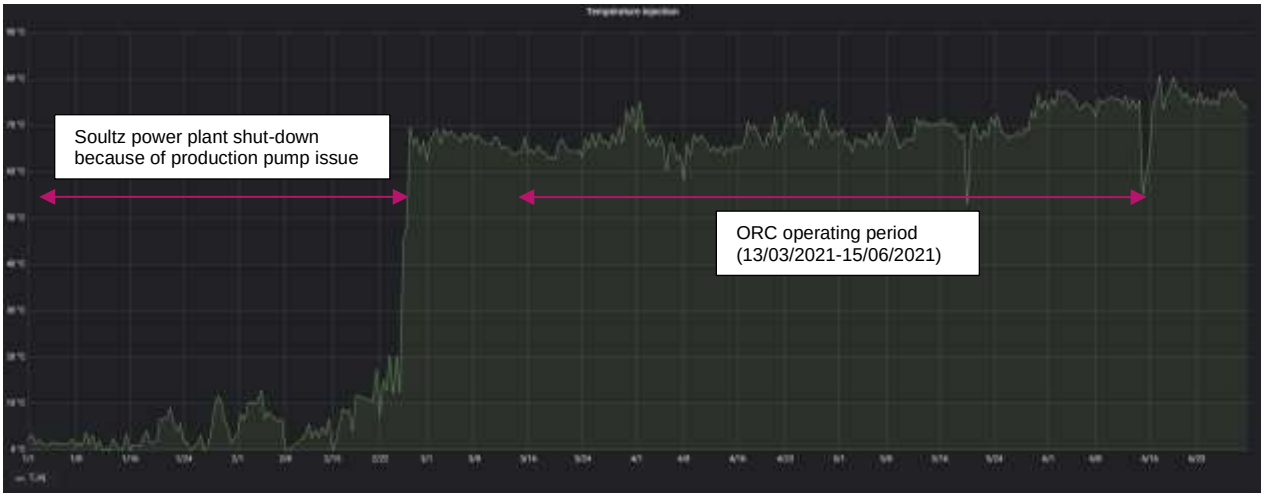

Figure 7: Reinjection temperature in Soultz between 01/01/2021 and 30/06/2021.

2.2.1.2 Cold water reinjection consequences derived from operation data

As the small-scale ORC did not result in a significant change in the injection temperature, it was decided to analyse the past operation dataset. As mentioned above, the main ORC efficiency has an impact on the injection temperature, as its efficiency changes with outdoor temperature. Thus, it was suspected that seasonal temperature changes have an impact on the reinjection temperature.

Indeed, this effect can be observed on the operation data, as the reinjection temperature changes between 55°C and 80°C (see Figure 8). The lower injection temperatures are observed in the winter times, when the ORC efficiency is the highest.

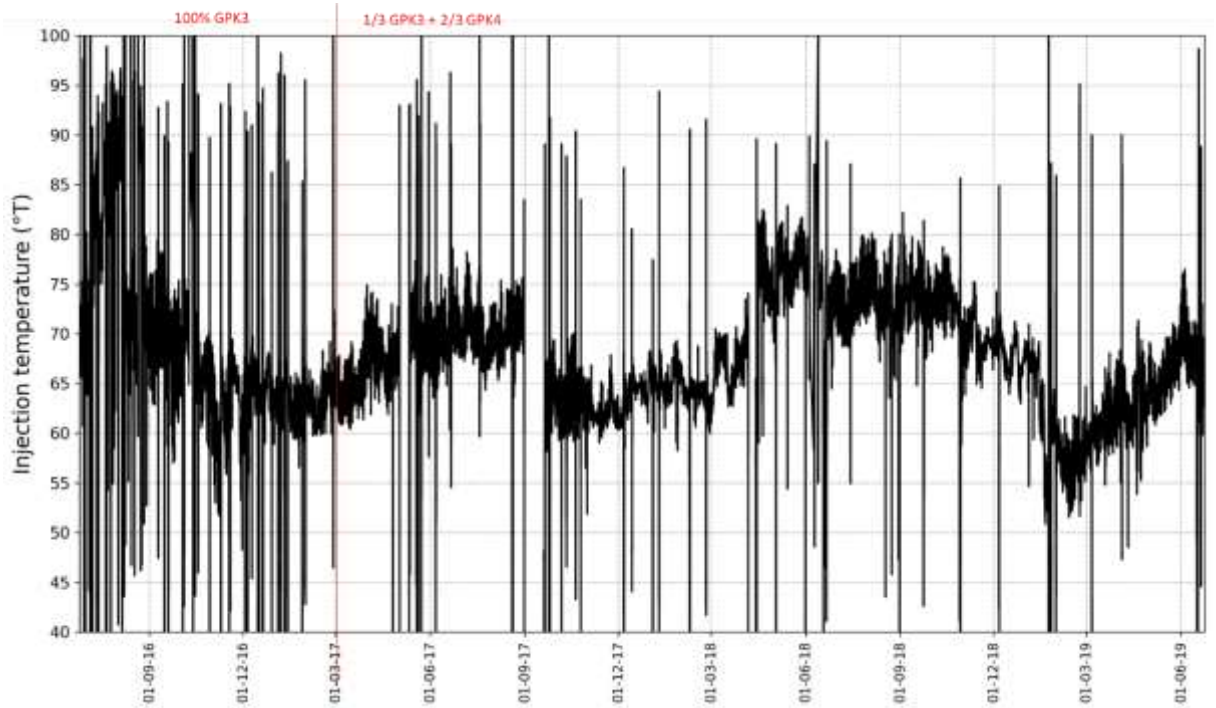

Figure 8: Reinjection temperature in Soultz in the model calibration dataset between 25/06/2016 and 24/06/2019.

Even if these variations are not very stable (as they depend on outdoor temperature, which is not controlled), the amplitude and the wavelength of these variations is sufficiently large to be taken into account for the model interpretations and to draw conclusions on the consequences of cold water reinjections in the reservoir (see also section 2.7).

A more detailed analysis of this dataset was carried out in order to investigate the relation between the injection temperature and the production temperature. To that purpose, production and injection temperatures over the available period was extracted and plotted (see Figure 9).

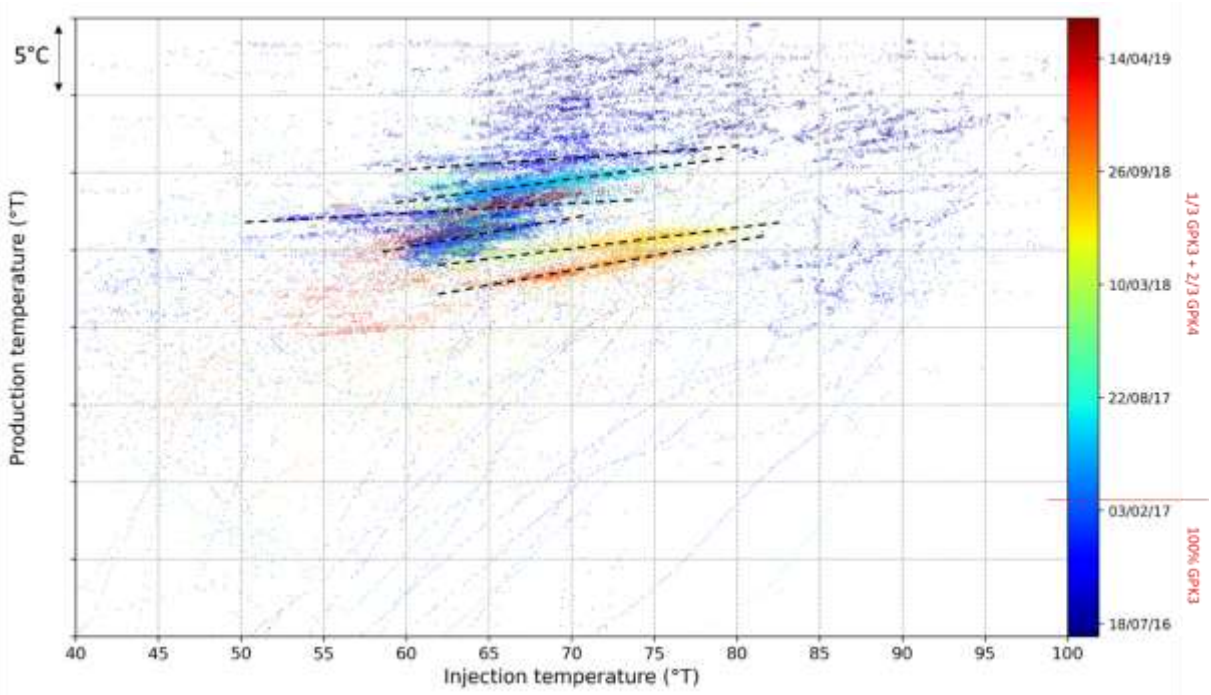

Figure 9: Relation of injection temperature with production temperature between 25/06/2016 and 24/06/2019. The absolute value of production temperature is hidden for confidentiality.

The following observations can be made on this plot:

- Globally, the average production temperature is decreasing with time (orange dots are lower than blue dots).
- At a constant rate (which is mostly the case) the production temperature should be constant and the injection temperature should vary according to the ORC efficiency, controlled by outdoor temperature. Therefore, at a given production temperature (controlled by flowrate), the points should follow a horizontal line.
- The points do not align on a horizontal line, but follow a slope. The slope is increasing with time, showing that the production temperature is somehow influenced by the injection temperature.

Thus, as the slope of the lines is increasing with time and as average production temperature is decreasing with time it can be concluded that there is a relation between

production temperature and injection temperature, indicating a thermal connection between the production well and injection wells in this particular case. Moreover, this connection is developing (as the slope is increasing with time); at the end of the period, an injection temperature decreases of 5°C seem to impact the production temperature of 1°C (slope of the line).

2.3 VSP AND 3D SEISMIC ANALYSIS

The original 3D geological model provided by ESG was used to build the main physical 3D models, namely the P-wave and S-wave velocity models as well as the density model, used to perform the FWM and Inversion (Full Wave Modelling and Inversion) applied to the VSP data. Then, these physical models were used as background seismic wave propagation to perform 2D and 3D simulations and inversions. After numerous numerical simulations, mainly in 2D, it was observed that a specific seismic feature observed in the real data could not be reproduced using these physical 3D models. The major limitation of the physical models is that the multipathing observation for the direct P-wave is not reproduced and then the observed data cannot be recovered.

This first observation shows that the initial geological model is not accurate enough to reproduce the observed seismic features. Therefore, it was decided to use the recently acquired 3D surface seismic (3DSS) concerning the same area, in order to build a more accurate stratigraphical and structural model, especially the top basement topography. 2D sections of this 3DSS had been kindly provided by ESG.

More precisely, 65 seismic lines had been extracted from the full 3D seismic cube and provided to GIM-labs: 31 in-lines oriented WNW-ESE and 34 cross-lines oriented NNE-SSW. We show on Figure 10 an example of the seismic data quality where the top basement interpretation (yellow curves) as well as the orthogonal projection of the main geothermal wells (GPK1 to 4 and EPS1).

The picking of the top basement was done by a step before the final interpretation. Once the picking of the in-lines was accomplished, we started to pick the top granites in the cross-lines (more difficult to interpret). Once both in- and cross-lines were picked, we performed a quality control (QC) to check the consistency between the picked interface in the in-lines and the cross-lines. This consistency was indicated on a numerical scale. Closer are the picked depths of the top of basement in the in-lines and cross-lines, higher is the quality indicator.

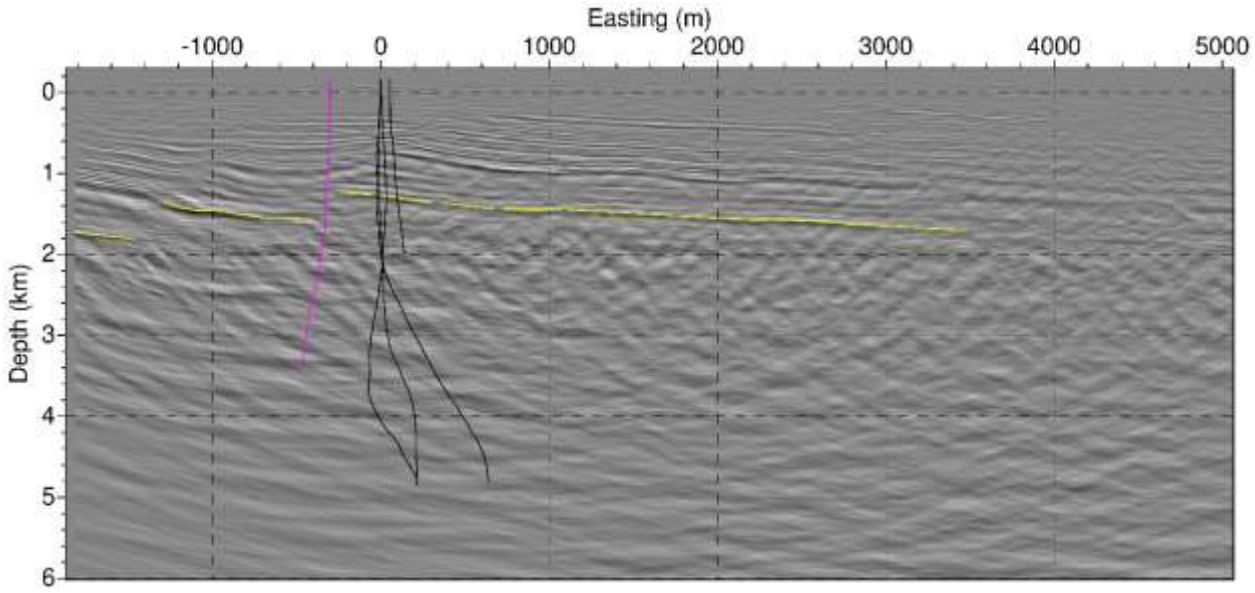

Figure 10: Seismic inline N 10339 crossing the GPK1 wellhead. The yellow curves show the interpretation of the top basement. We also show the orthogonal projection of the main geothermal well paths located in the area mainly GPK1 (purple), GPK2, GPK3, GPK4 and EPS1 (black lines).

The quality indicator is estimated in every point of the grid, thus defining a QC map. This map helps to define well picked regions (or simple ones) and errors in picking. We then checked and often picked again the seismic in order to improve the QC map. Several iterations were achieved to reach at the end an acceptable picking quality especially in the interesting areas located around the GPK's wells. However, some features appear in the QC map because some regions are difficult to pick due to discontinuities of the top basement. We showed on Figure 11 the final QC map obtained after several repicking iterations. We can see on this map that the picked top basement depth is constancy between the in- and cross-lines in the almost whole studied area, except in some specific zones. These zones can be observed in the western part of the wellheads, the zone located immediately in the western part of the Soultz horst.

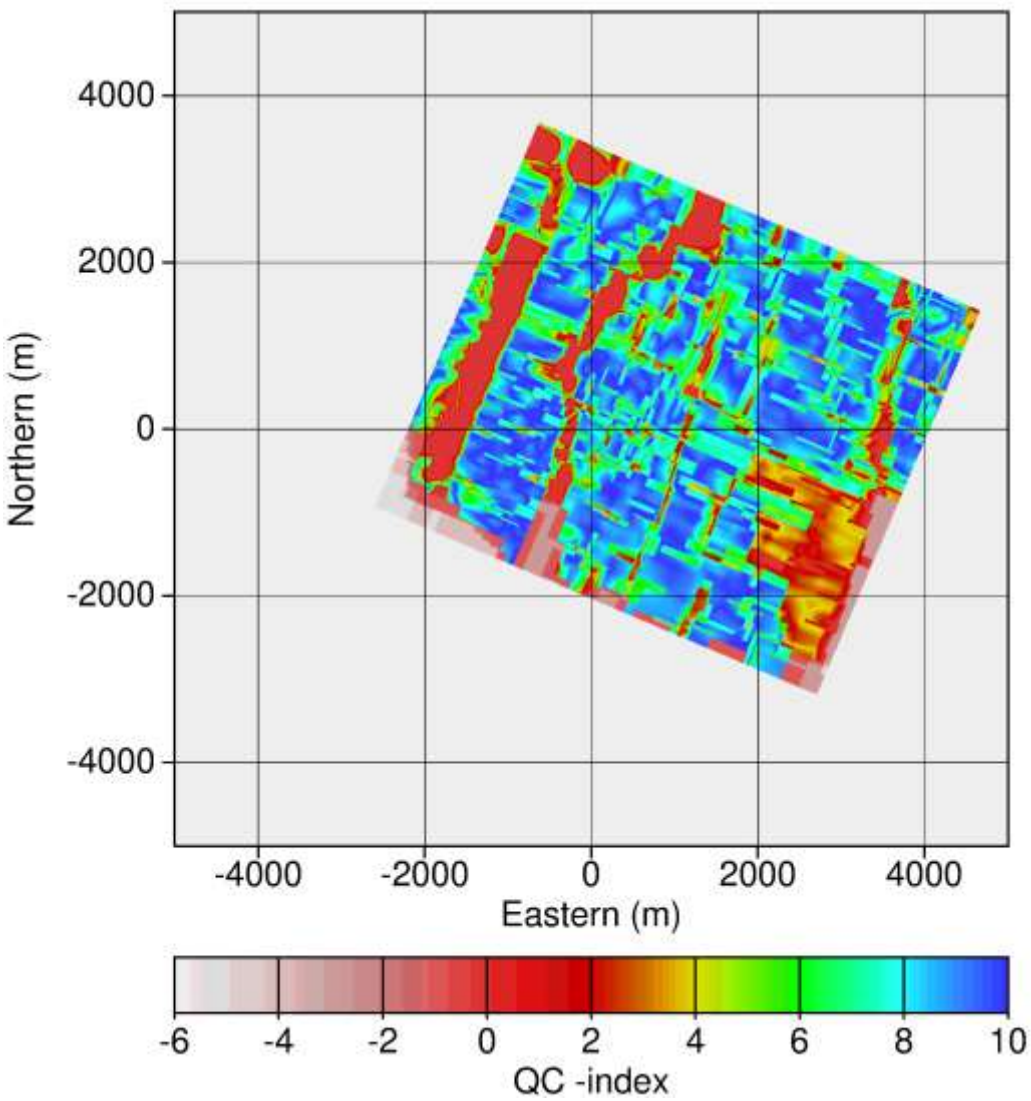

Figure 11: Surface seismic picking quality control. The depth of the picked top granite in the in-lines is compared to the depth picked in the cross-lines (from the nearest 2D profiles) and the Q-index is set according to the distance between the two depths. The QC indicator is perfect for 10, which means that the difference between the two depths is negligible regarding the wavelength of the seismic. The QC indicator -6 means "no data available". Between these two maximum and minimum values, negative QC values indicate missing data while positive values indicate discordance between picked depths. Between 0 and 2 important discordance or presence of a normal fault separating basement blocks, and between 6 and 8 show the areas of weak and interesting discordance as it revealed the fault network located at the top of the basement. The map origin (0, 0) is defined according to the GPK3 wellhead.

We can notice the presence of some interesting features on the QC map (Figure 11). These features are organized as straight structures which in some place correlate with known faults. These straight structures are detected in the top of the basement, but it could be continuous downward (information on the dip is difficult to obtain from the map and even from the seismic 2D profiles). The idea now is to extract the location of these lines from the QC map and incorporate them in the new top basement surface as in input information. We show in Figure 12 the raw version of the extracted faults, where we can

see that in some places, they match well with the abrupt topography chances of the top of the basement. The shape of the picked (raw) faults are now simplified in order to manage them and incorporate them in the final model as input.

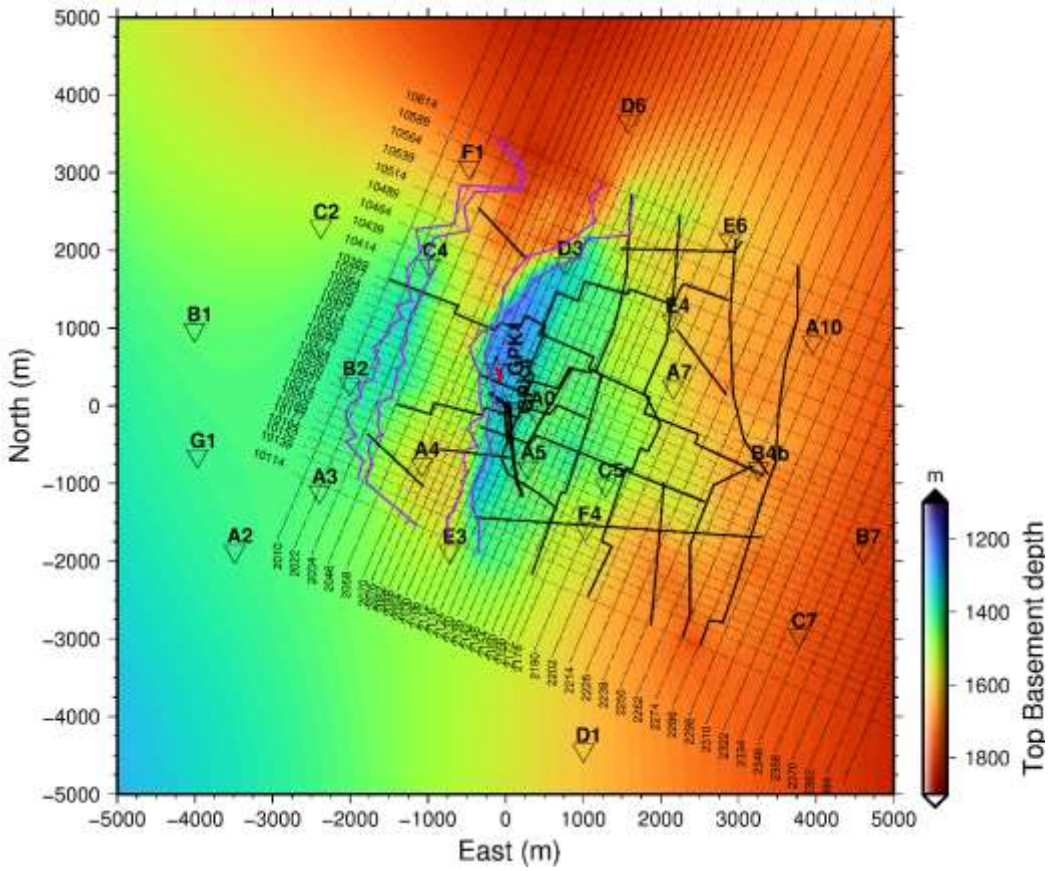

Figure 12: Top basement depth map in the studied zone. Faults located at the top of the basement extracted from seismic QC shown in Figure 11. The background is the new top basement obtained from the interpretation of the 3DSS. The seismic in- and cross-lines are also shown, as well as seismic sources and horizontal project of the borehole trajectories. Note that these faults are shown with some simplifications compared to that shown in Figure 11. The objective is to simplify these faults to model them numerically using equations. The purple curves show the lower part (left one) and the upper part (right one) of the fault forming the horst. The seismic sources for OVSP are shown by the invert triangles.

The fault's intersection defines blocks. These blocks could have different physical values which could explain the observed seismic features on the VSP data. Once the fault shapes are geologically corrected and simplified, the blocks are defined by fault's intersection. We show on Figure 13 a final blocked basement after incorporating the defined 35 blocks to the basement. These blocks are observed in the top of the basement, but the faults and block can extend in depth, deeper in the granites, but also upward in the sediments cover.

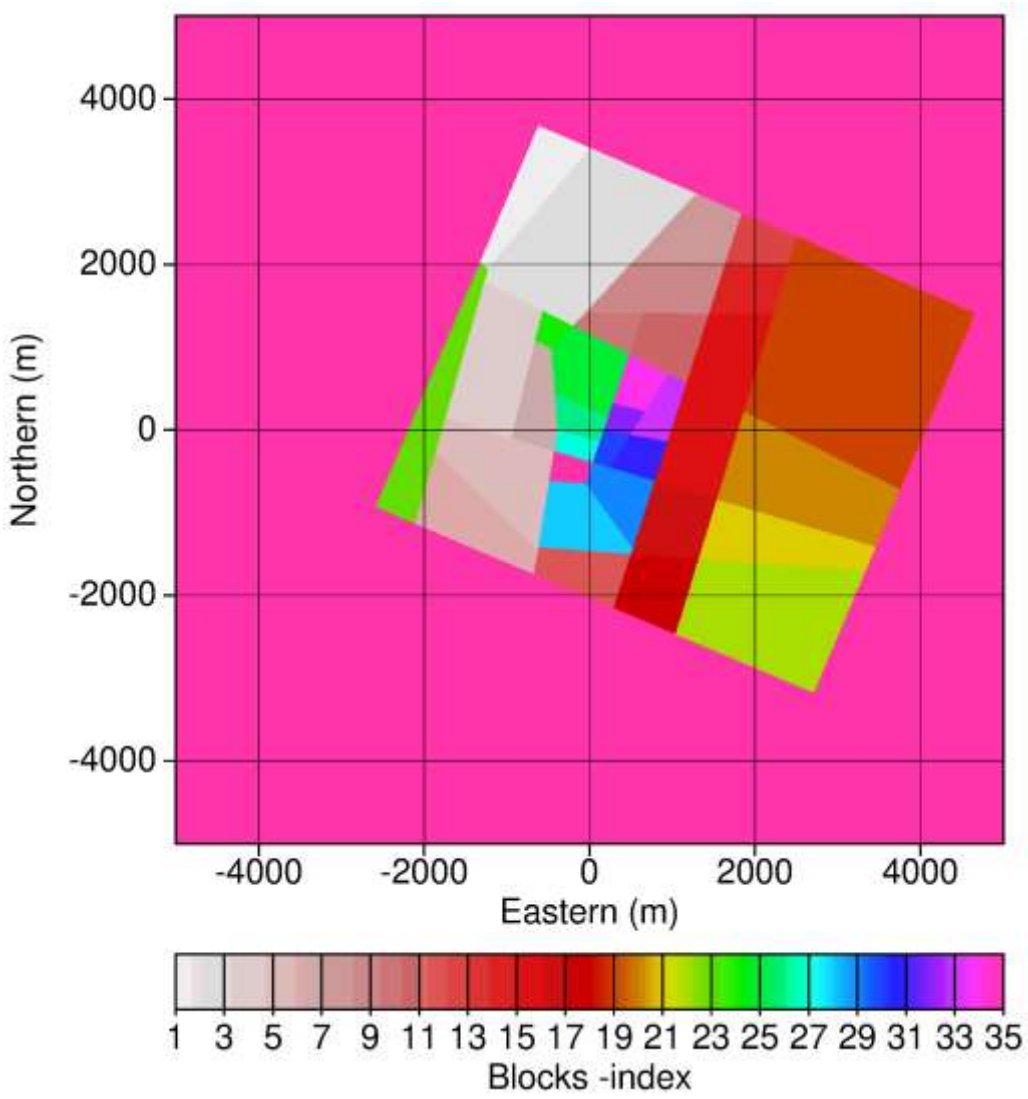

Figure 13: The simplified blocks adopted at the top of the basement, extracted from QC of surface seismic as shown in Figure 11. A total of 35 blocks are defined. The origin (0, 0) shows the location of the GPK3 wellhead. Notice that we focussed mainly on the blocks around the interesting area including the geothermal boreholes (i.e., GPK1-4) where more blocks details are included, whereas we simplified more the blocks outside the interesting area.

Once the top basement is accurately defined including the blocks, we merge the available surfaces to build an improved structural model and then define an improved physical models taking into account the basement zoned heterogeneities.

Several 3D FWM have been done on basis of the new version of the physical models. The idea is to quantify the seismic effect of each basement-block comparing the FWM results with the observed VSP data. We show for instance in Figure 14 the synthetic seismograms where the seismic effect of the block B2 was assessed resulting from 3D FWM using the improved physical models. The comparison to the non-blocked basement is also proposed where we can mainly see that the blocked basement provides a seismic wavefield qualitatively close to those observed in the real data. This conclusion means

that the 3D physical models built from the new top basement interface depth map taking into account more accurately the real geology in the study area. An important improvement was achieved on the structural and physical models.

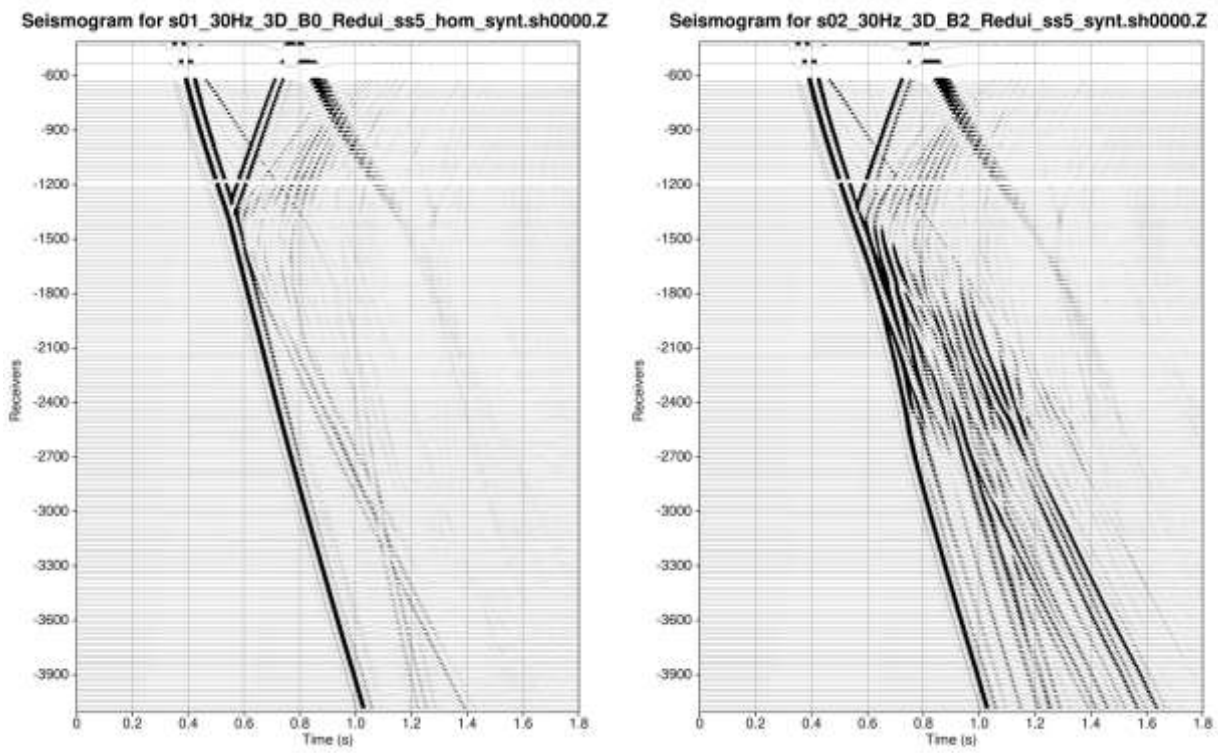

Figure 14: Synthetic seismograms for GPK4 obtained using 3D full-wave elastic modelling. The 1st seismogram is obtained for a non-blocky basement. The 2nd seismogram is obtained for a blocky basement, the block B2 velocities being lower.

2.4 HYDROTHERMAL RESERVOIR SIMULATIONS MODEL 1

This section presents an overview of the first modelling effort, realised in the framework of MEET WP3. For more details, please refer to MEET Deliverable 3.3 “Hydro-thermal model matching colder reinjection design” and to Baujard et al., 2021.

2.4.1 Workflow overview

This modelling work is based on the following workflow:

- A structural model was built in Petrel, based on 2D seismic and well interpretation data.
- Then, this model was simplified in order to keep only structure suspected to play a significant role in the hydrothermal behaviour of the Soultz reservoir. The reason of this step is that calculations are based on a finite element (FE) code, which needs an adequate mesh. As the meshing procedure is complex, and as the final element numbers is limited, this workflow cannot taking into account a high number of discrete features.

- The structural model was exported from Petrel and imported in MeshIt in order to build the 3D FE Mesh.
- The constructed FE Mesh was then exported from MeshIt and imported in FEFLOW for thermo-hydraulic simulations.
- The boundary conditions and initial state were defined in FEFLOW to reflect at best the reservoir conditions.
- The model was then parametrised, using the Soultz operation dataset as a calibration dataset for history matching.
- Simulations were carried out in FEFLOW according to different scenarios to calculate the extent and amplitude of the cooled-down reservoir volume and to predict the production temperature.

2.4.2 3D structural model

For this study, the model of Renard and Courrioux (1974) was chosen to be the initial data. The data of this model were available as 2D cross-sections. For each one, horizons were imported in Petrel as points. Then, each horizon has been linked between the different profiles in order to obtain a 3D structure. The wells trajectory GPK-1, GPK-2, GPK-3, GPK-4, EPS-1 and 4550 were also imported in the model. The two-mica granite layer (Place et al., 2010) has also been imported as a layer according to the depth in GPK-3 and GPK-4 where it was observed.
For each cross-section of the 1994 model, faults were imported as lines. Then, as for the horizons, they were associated to each other between the different profiles to obtain a 3D surface. The major sedimentary faults (Kutzenhausen, Soultz and Hermerswiller faults) were extended in the basement.

For the lower part of the structural model, information about faults were collected (Sausse et al., 2010 and Dezayes et al., 2010) thanks to different data:

- cuttings
- well logs including oriented borehole logs (caliper, gamma ray, Ultrasonic Borehole Imager)
- Vertical Seismic Profile (VSP)
- microseismicity studies

As a result, the constructed model is constituted by 6 geological layers. 50 structures representing local faults could be integrated in the Petrel model Figure 15. Each fault was added by informing its orientation and its dip in the table of the well which is intersected. Then in the 3D model, each fault identified in several wells was linked to create surfaces.

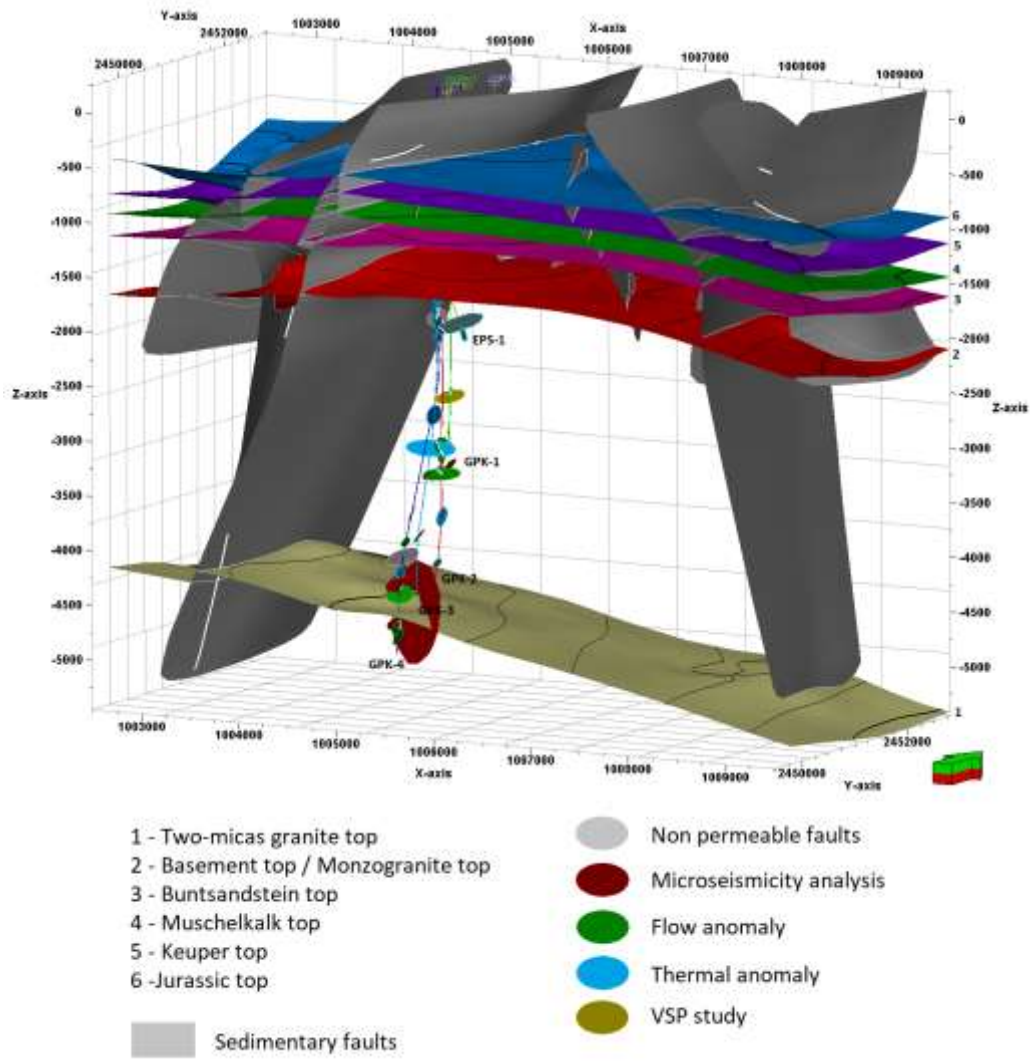

Figure 15: Complete 3D structural model of Soultz-sous-Forêts.

The model was then simplified in order to allow the finite element meshing workflow. The sedimentary faults are considered far enough from the wells to not have any influence on the simulations; therefore, it was decided to not keep them in the 3D hydrothermal model. To study the hydrothermal circulation in the granite and between wells, faults are selected on following criterions:

- Permeable faults: they must present flow or thermal anomalies, or have been detected by microseismicity cloud.
- Extension: they must intersect several wells to respect the connections between them.
- Contribution of the flow: recent flow logs and precedent studies allowed the estimation of the flow produced and injected in the different sections of the wells. In order to respect those contributions in the hydraulic calibration, it was necessary to keep faults crossing the well in specific sections.

The simplified final structural model is showed in Figure 16.

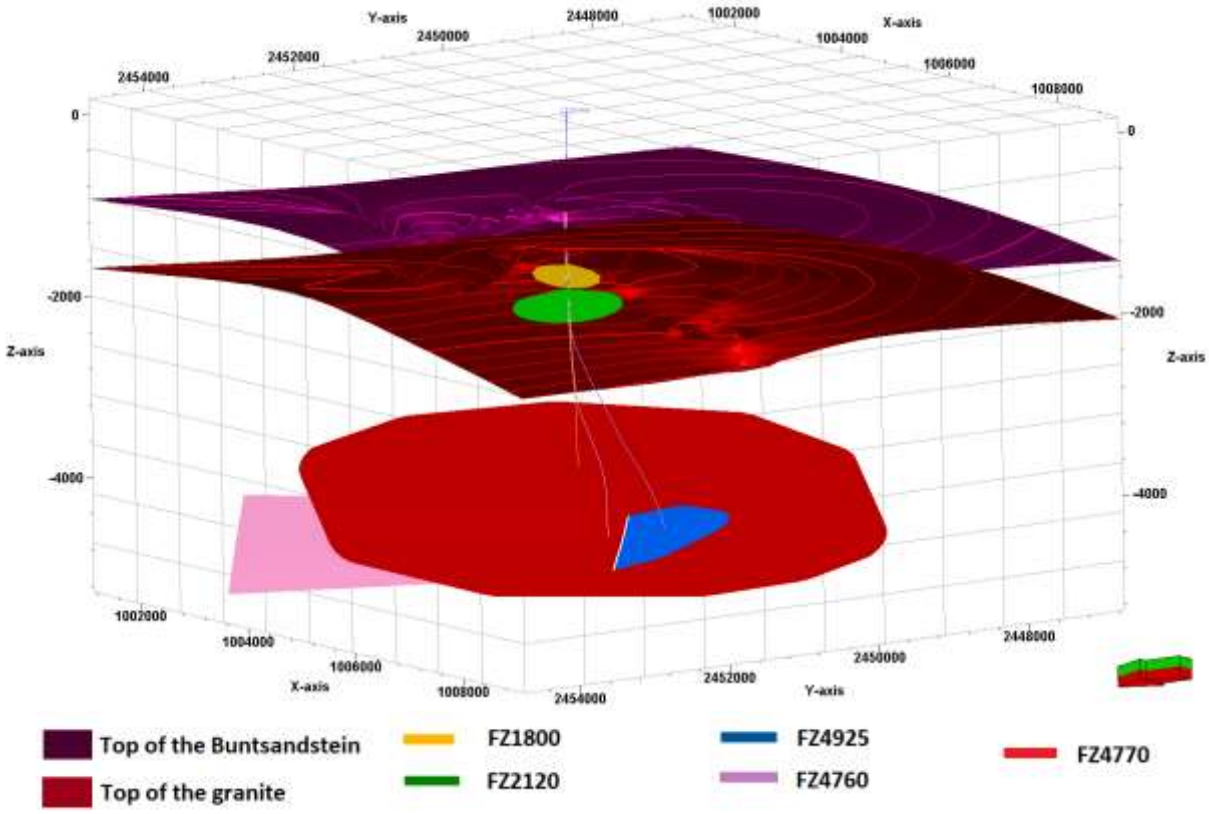

Figure 16: 3D structural model adapted to hydrothermal modelling.

2.4.3 Meshing of the model

The horizons and faults were extracted from Petrel as surfaces and imported in MeshIt, intermediate software which allows building units (Figure 17).

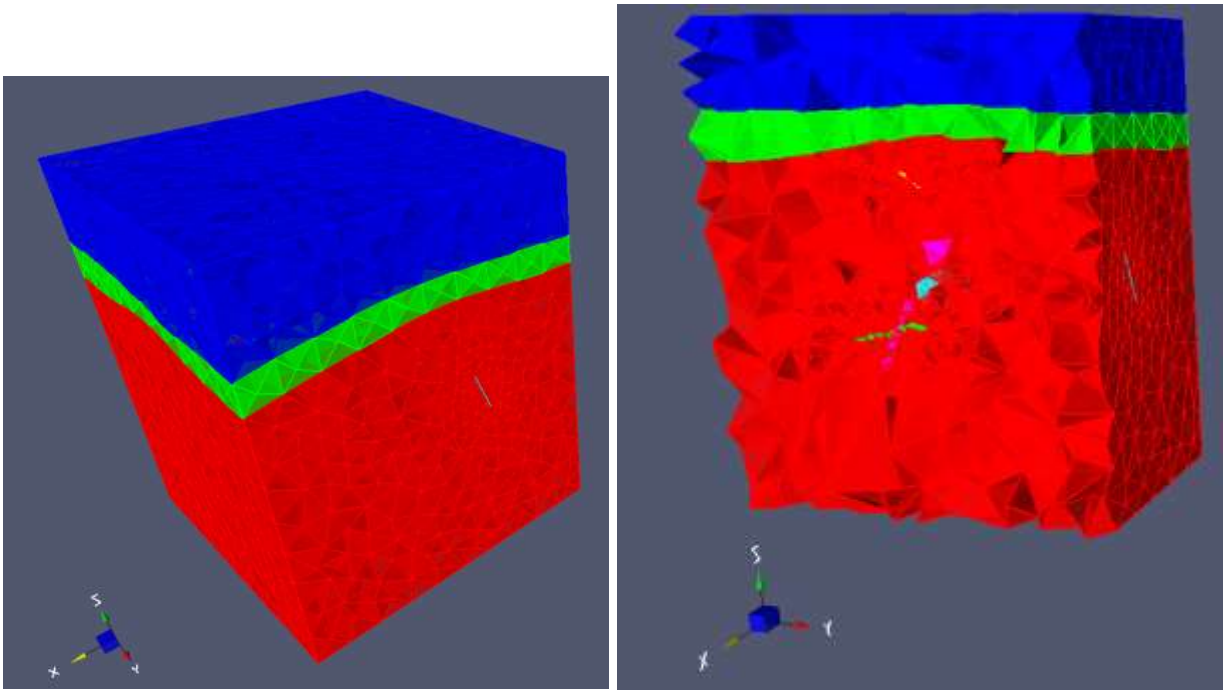

Figure 17: 3D structural model after meshing with MeshIt.

Once the model was structured, it was imported in to FEFLOW. The entire model was refined by the Tetgen algorithm, especially more precisely near the surface of faults where the distance between two points is 20 m and the wells trajectory where the refinement varies between 5 to 1 m near the intersection between faults and wells. It created an unstructured 3D tetrahedral mesh (Figure 18 and Figure 19). Faults were assigned to their corresponding surface as 2D discrete feature elements.

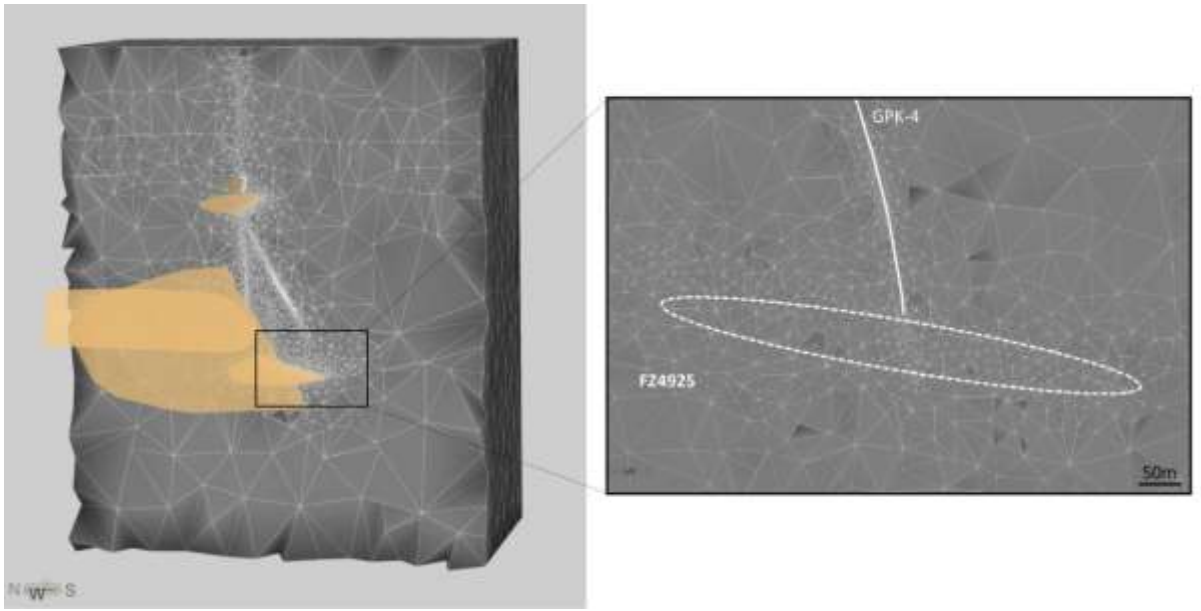

Figure 18: Meshing of the 3D structural model and zoom on the refinement meshing near GPK-4 and the fault FZ4925.

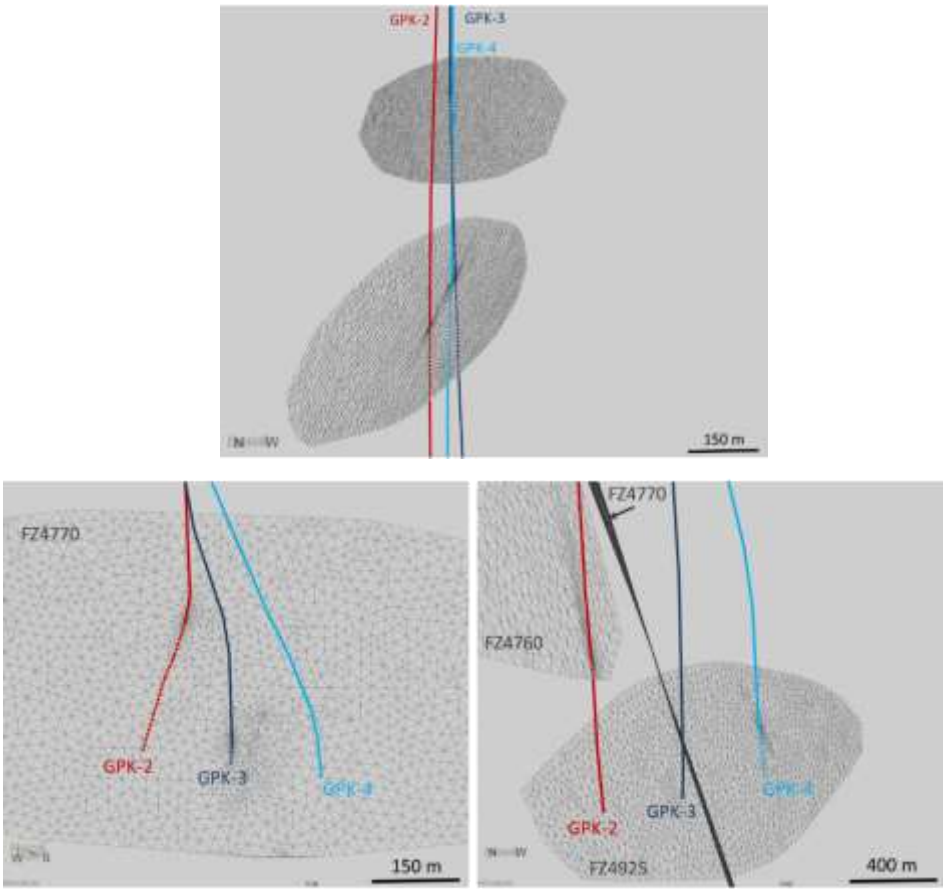

Figure 19: Zoom on the meshing of faults.

2.4.4 Hydrothermal processes, boundary conditions and initial state

The hydraulic calibration was solved in steady state without considering the heat transport. Then, the heat transport was added to calibrate the model in temperature. Firstly, the heat flow was solved in steady state to set the initial state of the simulations. Then, it was solved in transient state to calibrate the model to operation data. The final simulations were realized in full transient state.

The boundary conditions are defined as such:

- Constant hydraulic head of 10 m (= hydrostatic pressure gradient) boundary conditions on the lateral sides and on top of the model.
- A heat flux of 0.072 W/m² coming from the bottom of the model.
- The temperature is 10°C at the surface (0 m).

The initial state is defined by:

- A hydrostatic pressure gradient in the model.
- A non-linear temperature distribution, varying with depth. The measured temperature profile at the wells was imported as a temperature distribution. Calculations showed that this temperature profile remained almost unchanged over 50 years. Thus, within the timeframe of the simulation, the temperature distribution is representative to the

real temperature profile of GPK-3 during the 30 years of simulations discussed in this study.

2.4.5 Model Calibration

In order to calibrate the model, the hydraulic flow was solved in steady state. A flow rate of 30 L/s, 20 L/s and 10 L/s was attributed to GPK-2, GPK-3 and GPK-4. Their radius was set up to 0.12 m.

The calibration must respect:

- The estimated contribution of the fractures in each section of the wells (see Figure 3).
- The measured wellhead pressure during the past 3 years of operation: around 0 bar for GPK-2, 1 bar for GPK-3 and 18 bar for GPK-4 according to the flow rate attributed earlier.
- The production temperature observed in GPK-2, which is highly dependent on the preferential fluid flow paths governed by the relative hydraulic properties of the different fault zones (see Figure 4).

In the end, after an extensive sensitivity analysis, the contribution of the faults could be adequately reproduced. Similarly, well pressure and GPK-2 production temperature could also be acceptably fitted (see Figure 20). It is important to mention that the output GPK-2 production temperature from FEFLOW is a mean temperature from the different contributions. Therefore, it was necessary to correct the FEFLOW output to take into account the temperature losses in the well when the fluid circulates upwards over a few kilo-meters in the well in order to be able to compare the model results with observed temperature data (wellhead measurements). The temperature losses were calculated using a polynomial function of the flowrate and reservoir temperature, calculated using wellbore reservoir HEX-B for well GPK-2 (Megel et al., 2005). The same work was realized on the input injection temperature for GPK-3 and GPK-4 (i.e., the input temperature given to FEFLOW is higher than operation values as it takes into account the heating of the fluid when going down in the well).

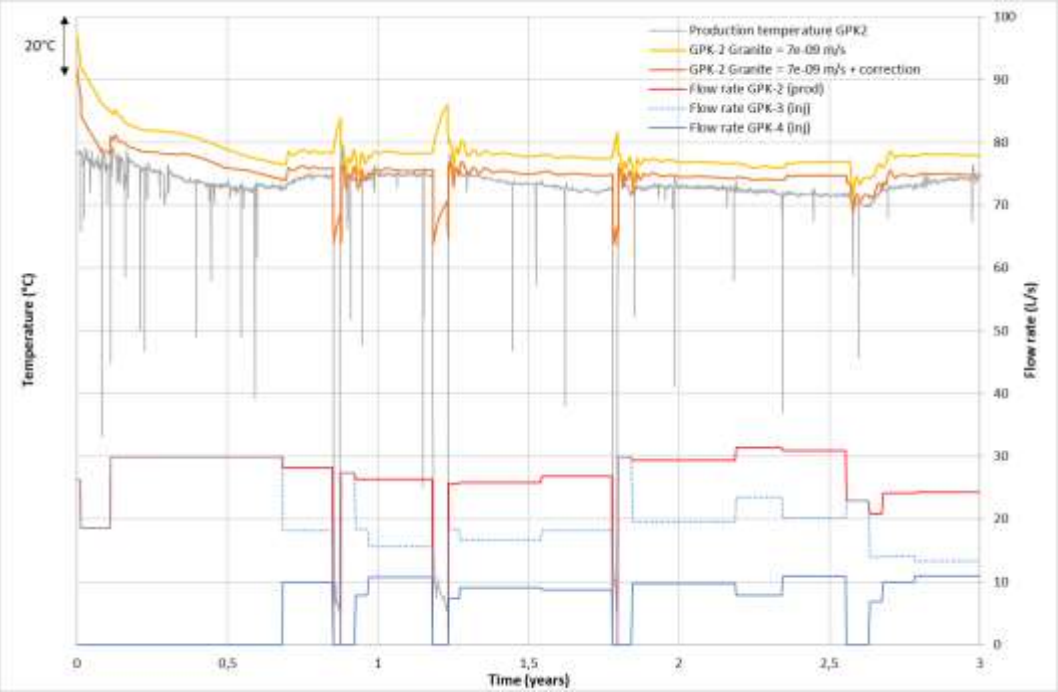

Figure 20: Comparison between simulated and operation data. The corrected value (orange line) takes into account the temperature losses in the well in order to be comparable to wellhead values.

2.4.6 Simulations and results

As the objective of the work is to estimate the variations of the production temperature over time in case of definitive decrease of the injection temperature and in case of a temporary decrease of the injection temperature, two scenarios were defined as following:

- The first scenario consists of following the first three years of operation and then changes of flow rates to 29.3 L/s for GPK-2, 19.6 L/s for GPK-3 and 9.7 L/s for GPK-4 (Figure 21). At the same time, the injection temperature is decreasing to 60°C, 50°C and 40°C for 30 years of simulation.
- The second one corresponds to follow the first three years of operation and then to decrease the injection temperature during 6 months to 60°C, 50°C and to 40°C while keeping the current flow rates to finally come back to 70°C of reinjection for the rest of the 30 years (Figure 22).

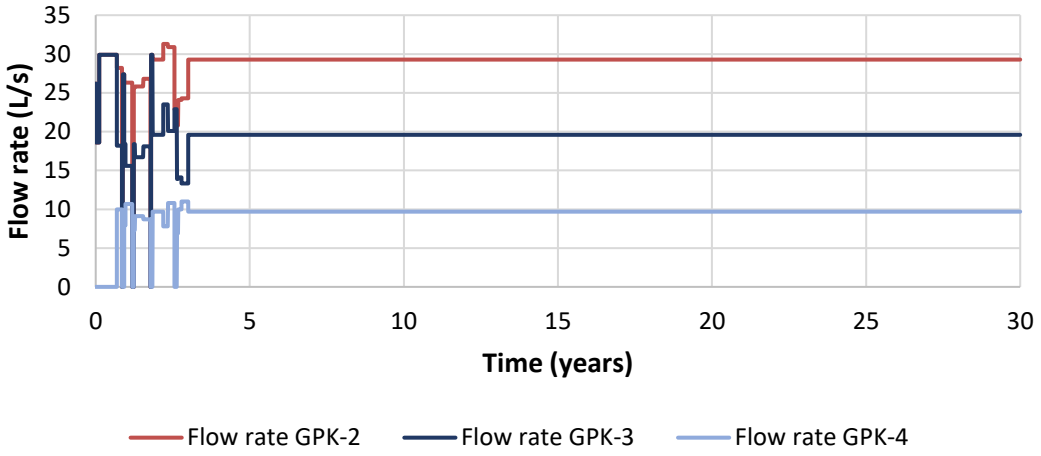

Figure 21: Flow rates attributed to each well (GPK-2, GPK-3 and GPK-4) during simulation of scenario 1.

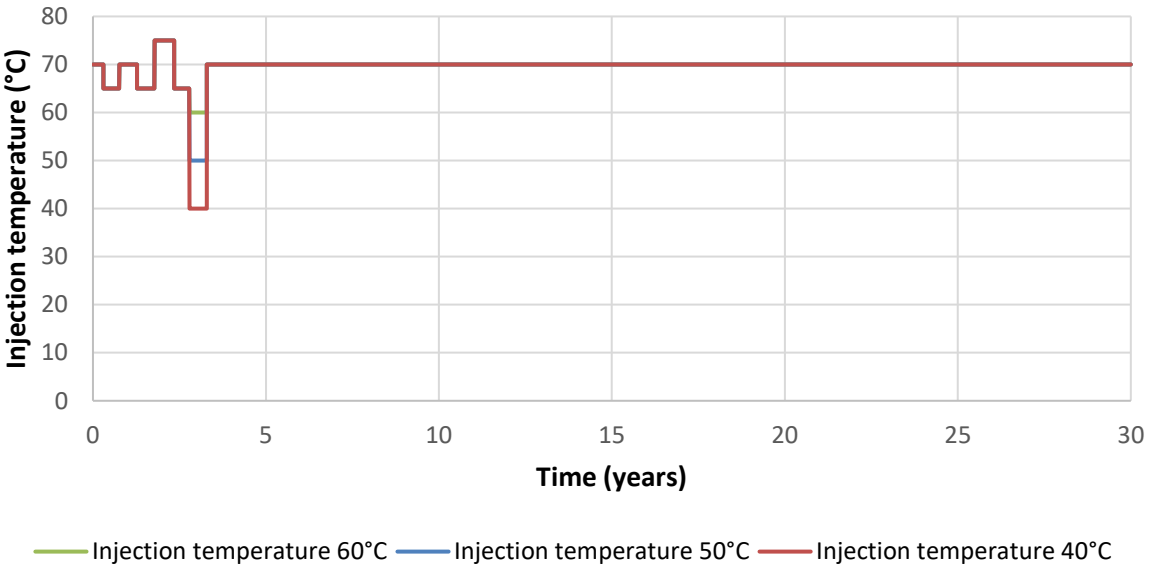

Figure 22: Temperature of reinjection imposed in the scenario 2.

2.4.6.1 Scenario 1

This scenario assumes a definitive temperature decrease of injection temperature. Four cases were tested corresponding to each reinjection temperature of 70°C, 60°C, 50°C and 40 °C. Over time, the thermal front is spreading into the reservoir from injection wells to reach the production well GPK-2 (Figure 23). The lower the reinjection temperature is, the faster the colder front propagates (Figure 24). In this case, the drop of temperature begins 6 months after the end of operation data and beginning of reinjection at 70°C, 60°C, 50°C and 40°C (Figure 25).

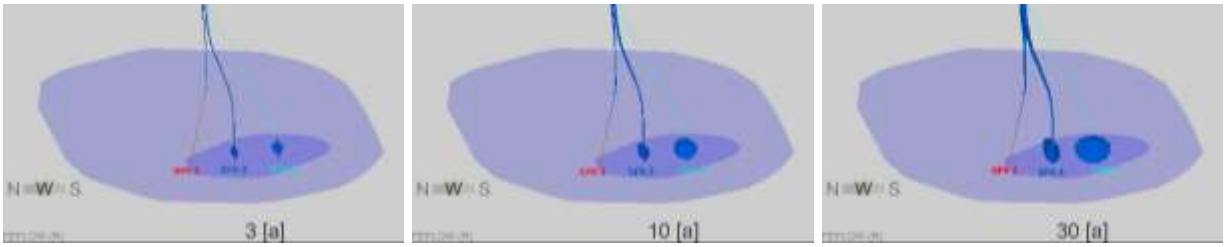

Figure 23: Evolution of the 130°C thermal front over 30 years in the case of a reinjection at 40°C.

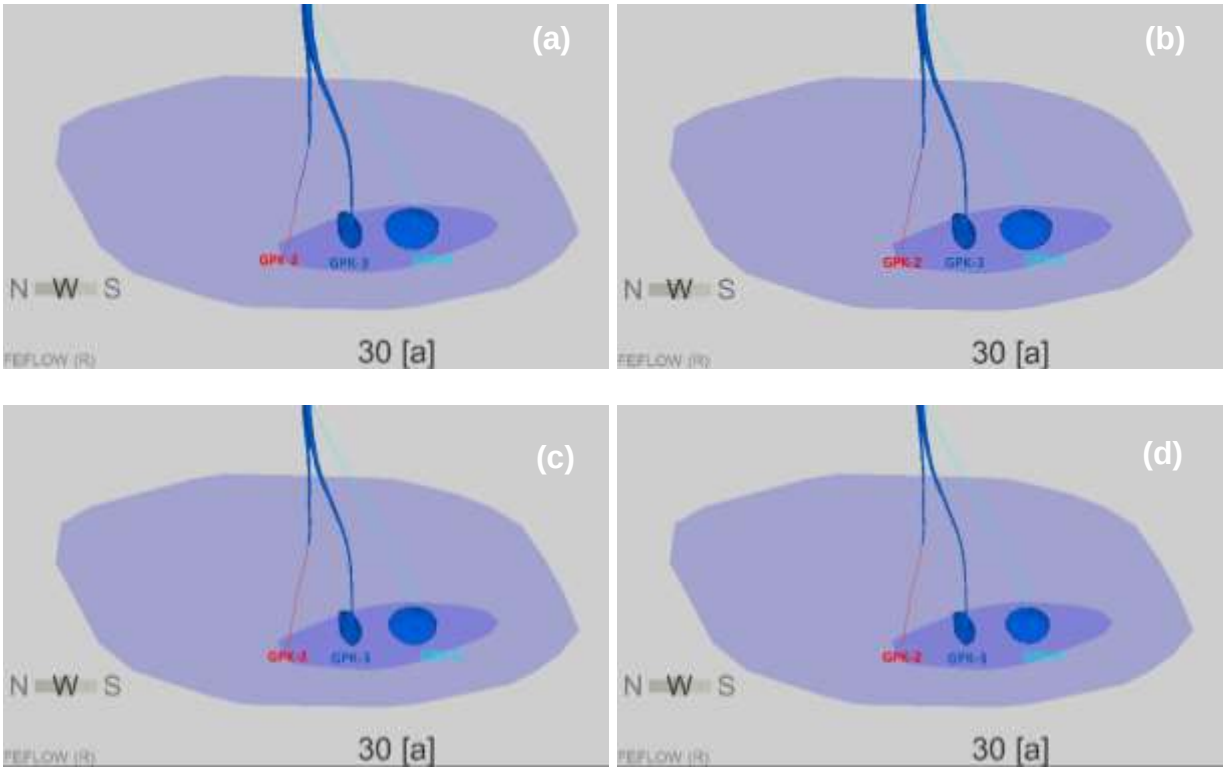

Figure 24: Spreading of the thermal front according to the injection temperature (a) 40°C, (b) 50°C, (c) 60°C (d) 70°C after 30 years of simulation.

The results show that a decrease of 10 °C in the injection temperature in GPK-3 and GPK-4 is expected to produce a drop of approximately 2.8 °C on production temperature at GPK-2 over 30 years. It is interesting to note that this drop does not increase significantly with time, as the drop is already significant (2 °C) after 2 years operation (i.e., after 5 years simulation).

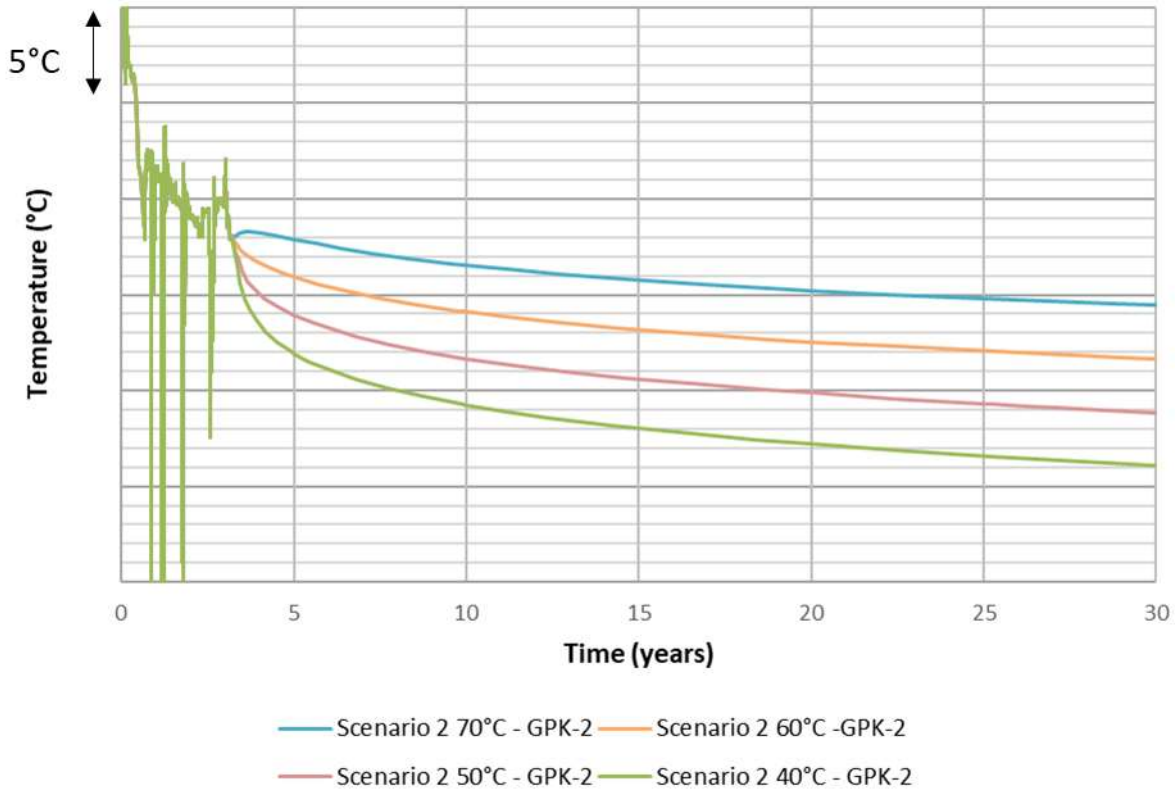

Figure 25: Production temperature for each reinjection temperature during the scenario 2 simulation. Absolute values of temperature are hidden for confidentiality.

2.4.6.2 Scenario 2

The 2nd scenario tested a reinjection over short time, here 6 months in order to estimate how long the system take to come back to equilibrium. The flow rates taken were the last one of the operation data. Figure 26 presents the results of the scenario 2. The arrow 0 shows the beginning of colder reinjection. The 1 corresponds to the beginning of the temperature drop at 3.25 years. The 2 is the minimum temperature of production obtained. The 3 marks the beginning of the second level of the curve as the come back to equilibrium is done in two phases. The number 4 is showing the moment where all the curves have recovered an equilibrium state.

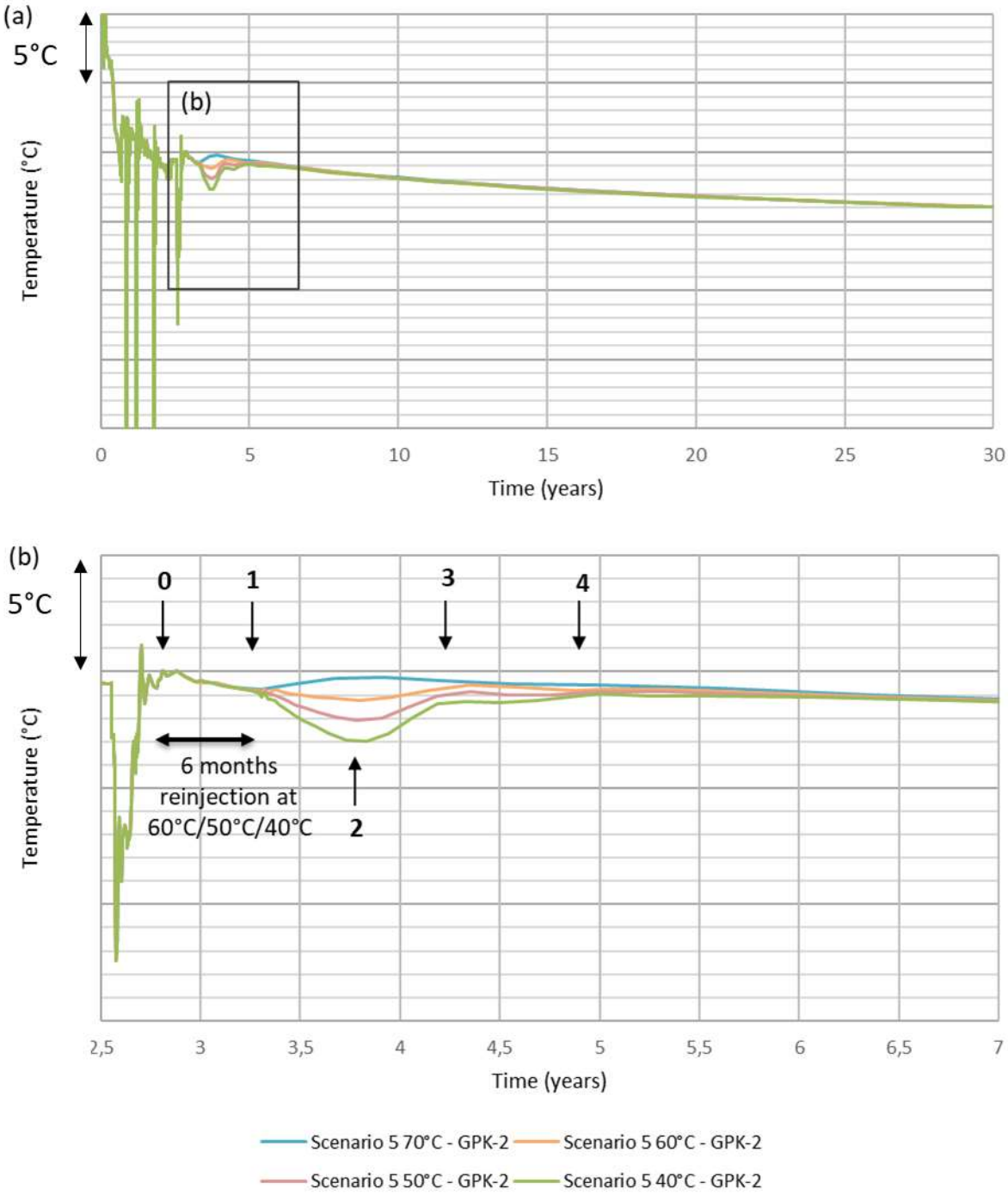

Figure 26: (a) Production temperature obtained for each injection temperature during the scenario 2 simulation. (b) Zoom on period after 6 months of reinjection. Absolute values of temperature are hidden for confidentiality.

The production temperature is impacted by the reinjection about 6 months after the beginning of the test. The maximum temperature difference is obtained around one year after the beginning of the colder reinjection. Zooming on the period around colder reinjection (Figure 26), the colder the reinjection is, the longer the model takes to return to equilibrium production temperature.

Interestingly, the production temperature recovery is done in two steps. At first, the temperature recovery is relatively fast over about 6 months, and then, the temperature recovery continues at a lower rate, mainly for colder reinjections temperature.

The effect of the temporary colder reinjection disappears about between one year (reinjection at 60°C) and 1.5 year ((reinjection at 40°C and 50°C) after the end of the colder reinjections.

2.5 HYDROTHERMAL RESERVOIR SIMULATIONS MODEL 2

2.5.1 Workflow overview

This modelling work is based on the following workflow:

- The structural model was built in Petrel. This model is based on VSP analysis, 3D seismic interpretation results and well interpretation data. This, the structural model is much more detailed and realistic than the previous one.
- No simplification of the structural model was carried out.
- Based on the structural model, a finite difference grid was built in Petrel, including the fault zones as 3D cells.
- The grid was then exported to be used in the pre-processing software Re-Studio to prepare the Eclipse simulations, and define the boundary conditions and initial state.
- The model was then parametrised, using the Soultz operation dataset as a calibration dataset for history matching.
- Simulations were carried out in Eclipse according to different scenarios to calculate the extent and amplitude of the cooled-down reservoir volume and to predict the production temperature.

Thus, the main improvement of this model is related to the structural model. The calculations were realised with Eclipse. The Eclipse simulation code, widely used in the oil and gas industry is very different from FEFLOW, as it is a finite difference code primary destinated to porous media. This code chosen in order to evaluate the flexibility of use of such codes as well as the confidence in the results one could have on this kind of codes for geothermal use.

2.5.2 3D structural model

The calibration of the first model showed the limitations of the structural model behind the simulations. Indeed, it appeared necessary to extend one of the faults (FZ4760) to the boundary of the model and to attribute to this structure higher transmissivity values than inferred during the hydraulic tests of the well, in order to get far-field contribution from the reservoir to the system. It is possible that the hydraulic properties of this fault increase with time since testing, as mentioned previously, but this possibly shows that some of the faults included in the model could be connected to great extension structures like the Soultz horst border faults which have at least 500 m of vertical offset that connect the system to the regional geothermal reservoir.

In 2018, Electricité de Strasbourg conducted a 3D seismic acquisition survey (Richard et al., 2021). This seismic acquisition covered the Soultz-sous-Forêts wells and reservoir.

Available vintage VSP data and this 3D seismic data were reprocessed and reinterpreted in the framework of MEET (see section 2.3).

Thus, it was decided to update the local Soultz structural model by considering these new results. On the new light of these data, some faults in the granite included in the model, derived from imaging well data are connected to regional scale structures (see Figure 21Figure 27), especially in the upper part of the reservoir (1500 – 2500 m – for example FZ2120). This could possibly validate the contribution of the far-field to the Soultz hydraulic system through the upper part of the reservoir or, on the contrary, show that additional connections to the far-field do exist in the deep reservoir, but could not be seen on the 3D seismic data.

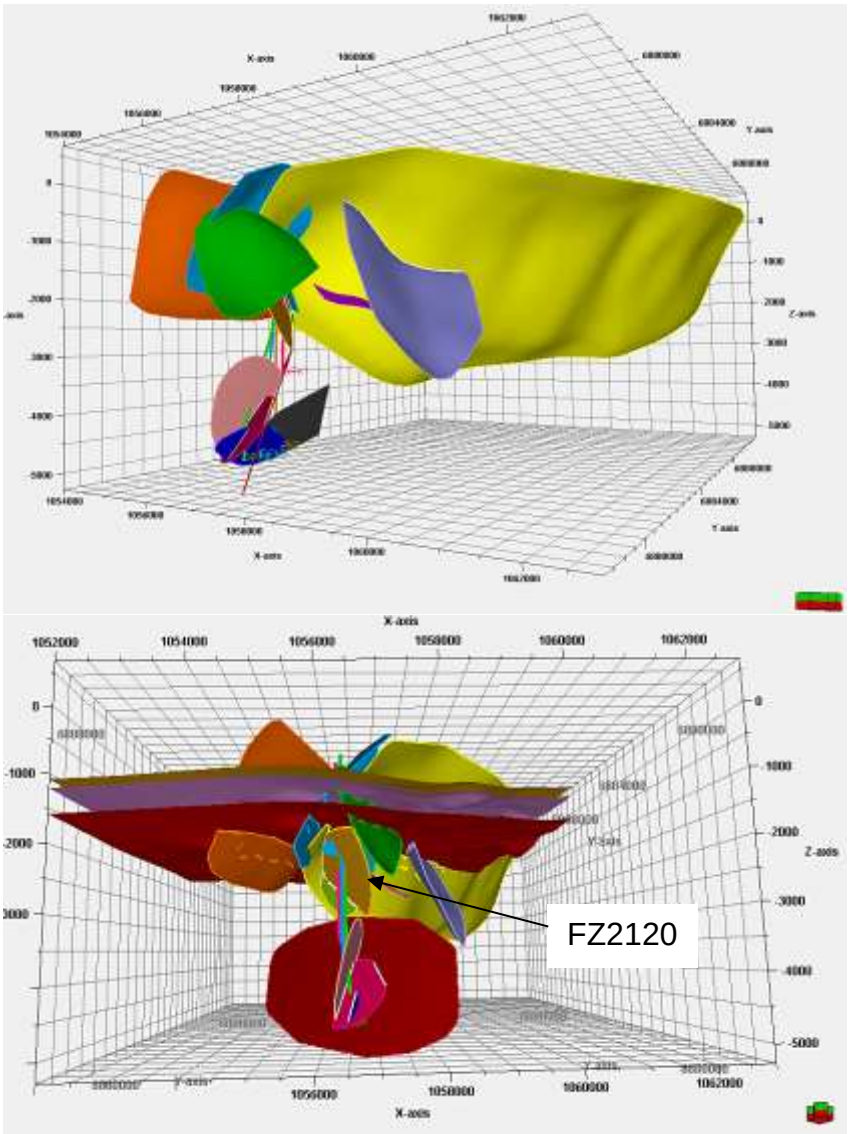

Figure 27: Updated structural model. On top: the image shows the new regional faults on the upper part of the reservoir (yellow, orange, blue, green and violet structures) and faults in the deep reservoir. On bottom: the image shows the same new regional faults, the new horizons top Muschelkalk (brown), top Buntsandstein (pink) and top Granite (red) and the new structural fault model in the granite.

2.5.3 Gridding process

A corner point Grid was built to convert the Petrel model into a grid of cells that can be imported by Eclipse. The grid in Corner point format has been structured in cells with (80, 80, 50) along the XYZ axes. The final grid is constituted by 320,000 cells. Faults are included in the grid as stair-step cell structures (Figure 28).

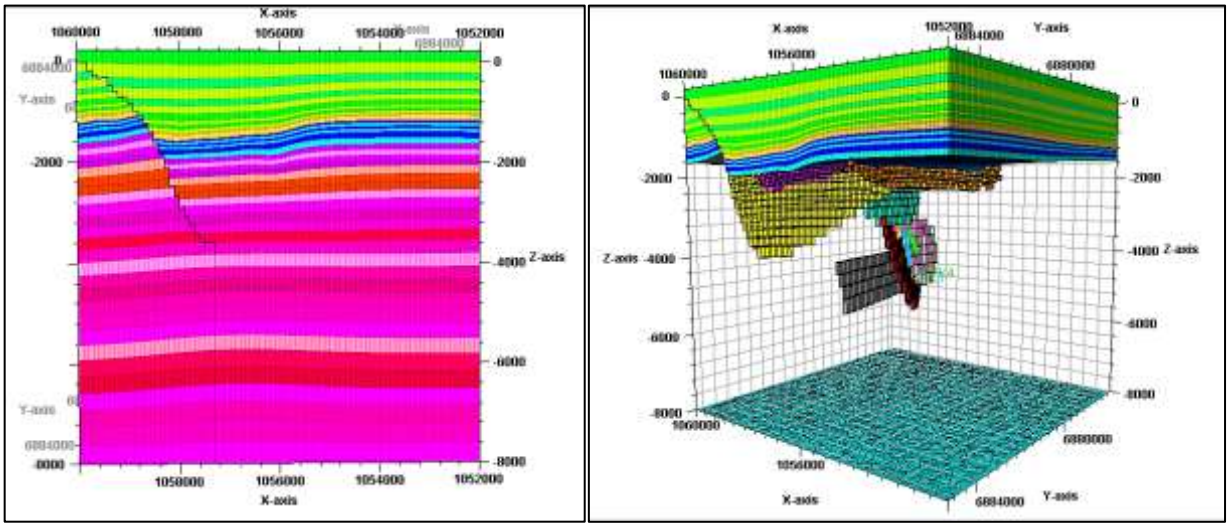

Figure 28: Corner point grid built from the Petrel structural model for Eclipse. Left: East-West cross-section of the grid. Right: 3D view of the grid. The granite cells are hidden to show the faults.

The gridding workflow is quite straight forward and allows on-the-fly modifications of the structural model to be taken in account in the grid. Thus, on the contrary to the finite element mesh used with FEFLOW, this approach allows to test the sensitivity of the structural assumptions behind the model.

2.5.4 Hydrothermal processes, initial state and boundary conditions

The calculations were run transient for hydraulic and heat transport.

The boundary conditions are defined as such:

- Open boundary conditions on the lateral sides.
- Constant pressure at the surface (1 bar).

The initial state is defined by:

- A hydrostatic pressure gradient in the model.
- A non-linear temperature distribution, varying with depth.

2.5.5 Model Calibration

The sensitivity study showed that increasing the multiplicative coefficient of fault transmissibility varies the production temperature of the GPK-2 well. However, Eclipse was unable to perform the calculations for values above 20 of the transmissibility coefficients (TR). However, some faults were sensitive to an increase in production temperature in GPK-2 (GPK-2_FZ2120; GPK-1_EPS_1200; GPK-1_FZ1820) while

others created a decrease in temperature. Thus, the best fit is obtained when the transmissibility coefficient is increased for faults creating a decrease in production temperature (GPK-2_FZ4760; GPK-3_FZ4770 and GPK-4_FZ4925). It comes out from the sensitivity analysis that the GPK-4_FZ4925 fault is more sensitive to temperature decrease.

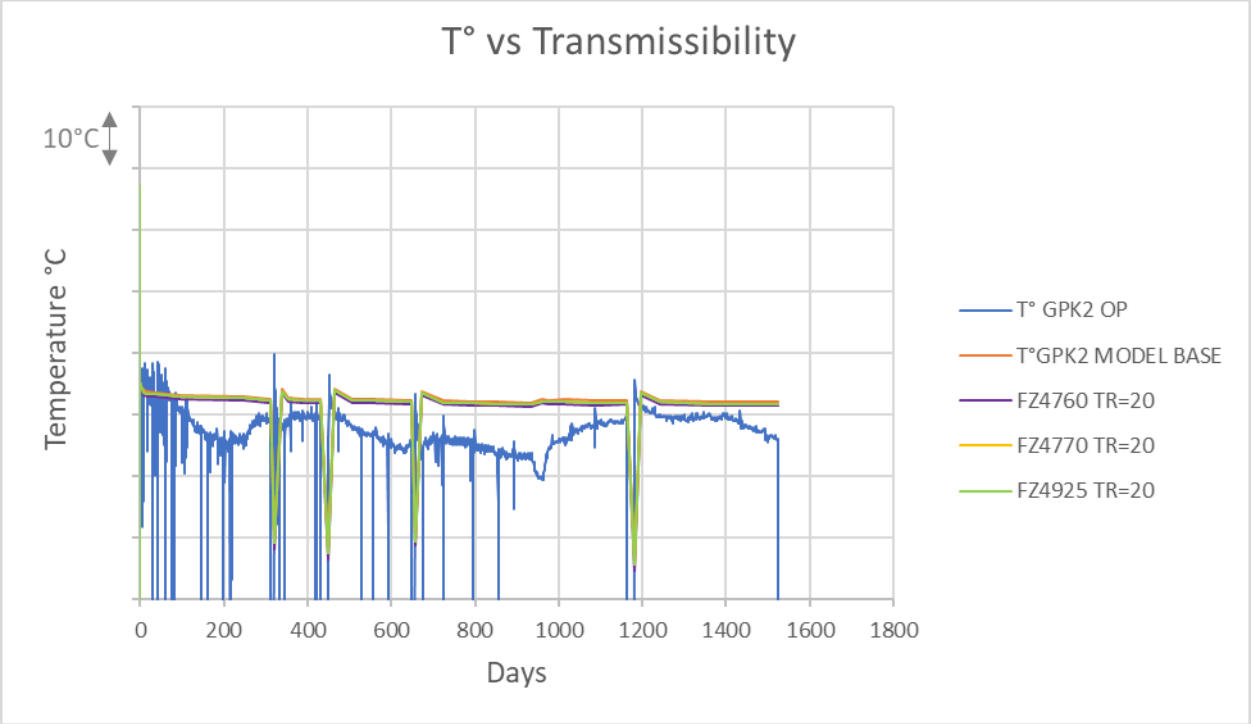

Figure 29: Comparison of faults sensitivities to temperature decrease.

It must be pointed out that the model output is representative from a downhole temperature, whereas operation data show wellhead data. The wellhead temperature is estimated to be between 3 and 5°C lower than downhole temperature, because of cooling down of the fluid upwards in the well (Figure 29).

2.5.6 Simulations and results

The respective reinjection rates of GPK-3 and GPK-4 are 19.6 L/s (1693.44 m^3/day) and 9.7 L/s (838.08 m^3/day). And the production of GPK-2 is estimated at 29.3 L/s (2531.52 m^3/day) (see Figure 30). In order to evaluate the impact on the production temperature of the colder reinjection tests planned at Soultz-sous-Forêts from year 2022 onwards, four scenarios were simulated with a decreasing variation of the reinjection temperature.

- Scenario 1: reinjection at 70°C.
- Scenario 2: reinjection at 60°C.
- Scenario 3: reinjection at 50°C.
- Scenario 4: reinjection at 40°C.

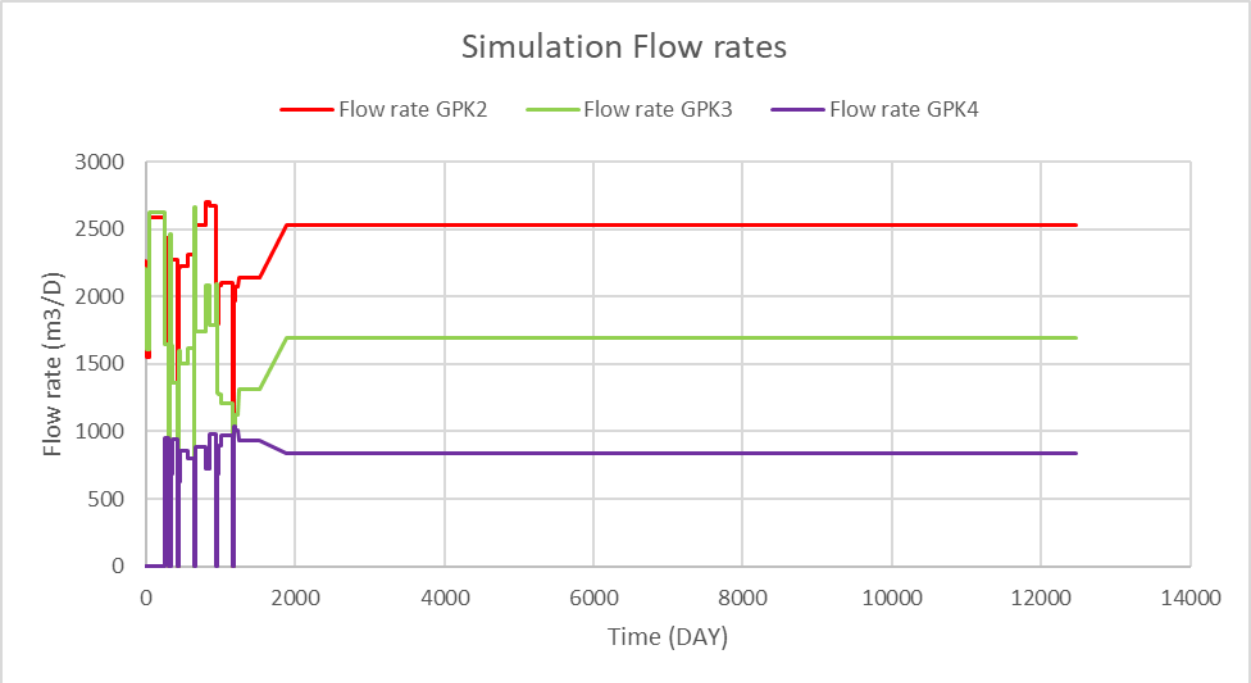

Figure 30: Simulation flow rates.

The first observation made in the simulations is that the production temperature of GPK-2 decreases over time. This confirms the connections that exist between the wells in the model due to the faults. However, some faults are more sensitive than others to this cold-water propagation which will affect production in the long term. The most sensitive faults are GPK-2_FZ4760, GPK-3_FZ4770 and GPK-4_FZ4925.

The superposition of the temperature curves of GPK-2 at different production temperatures shows that the cold water does not reach the well immediately (see Figure 31). This period of stability lasts about 4 years after the last measurements in year 2020, i.e., the effect of the cooling will only be felt in year 2024. The production temperature of GPK-2 in year 2020, which is around 151°C, will then fall by around 6°C in year 2050 if reinjection takes place at 40°C.

It must be pointed out that the temperature decrease calculated for a reinjection at 70 °C is quite similar with model 1, but appears to be much smaller for lower injection temperatures than the decrease predicted by model 1. This is possibly due to a more detailed structural model. But this could also be due to some limitations in the use of Eclipse. Indeed, the code was unable to perform the calculations for values above 20 for the fault transmissibility coefficients, thus limiting the hydraulic role of faults in the reservoir flow model. This is likely due to an inappropriate grid use; more refinement would be needed in the vicinity of the faults but this was not possible because of insufficient pre-processing software capabilities.

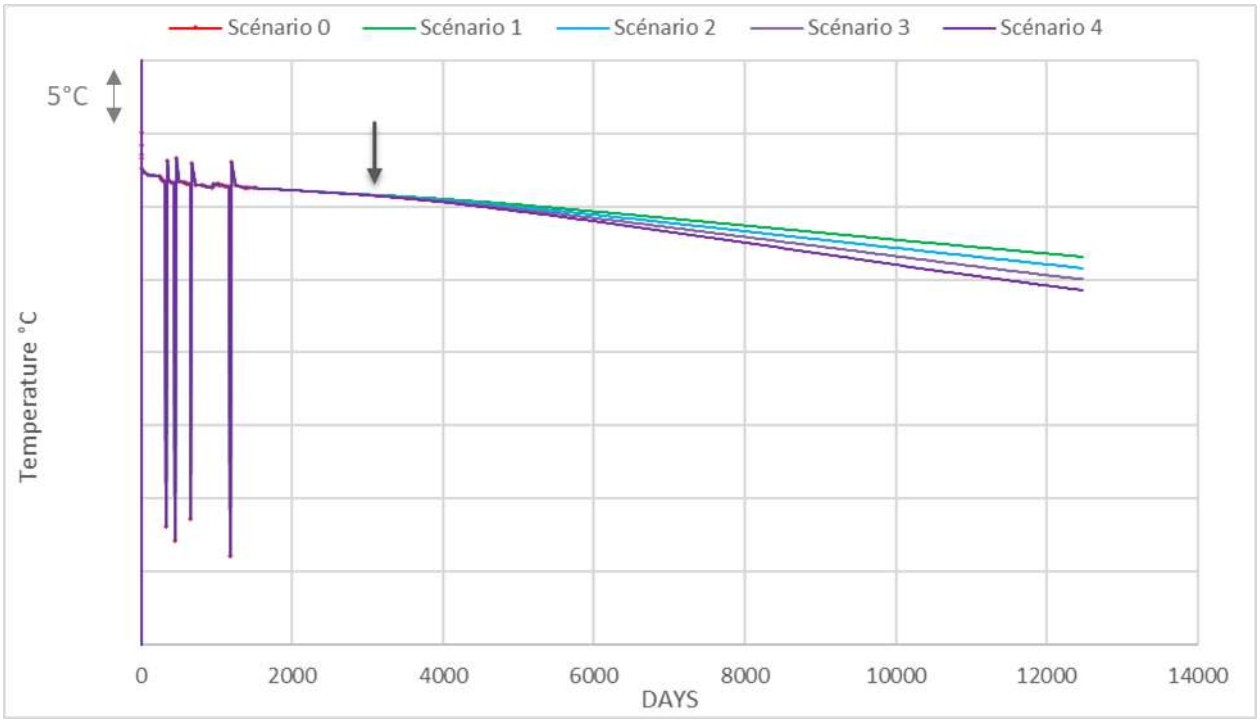

Figure 31: Temperature of GPK-2 according to scenario 1 - 4. As mentioned, the temperature effect in this model is very likely due to an inappropriate grid used for the calculations, thus limiting the fault contributions to the reservoir flow.

Concerning the methodology, as a result, it appears that the use of Eclipse in combination with the pre-processing software Re-Studio does not offer adequate options, as several limitations were identified during this work, such as the limited gridding process capabilities, permeability limitations, and not existing open hydraulic boundary conditions. Nevertheless, as mentioned, the structural model could be confirmed using these calculations, as the calibration process could fit the operation data over the history matching phase.

2.6 HYDROTHERMAL RESERVOIR SIMULATIONS MODEL 3

2.6.1 Workflow overview

First it presents a brief geological setting of Soultz-Sous-Forêts, followed by numerical modelling studies for the site. Furthermore, the mathematical and computational technique to model hydro-thermal processes during heat mining from a fractured reservoir is discussed. Next, the wellbore-reservoir coupling is demonstrated and its impact on wellhead temperature is quantified. In the following section, model results on different colder reinjection scenario and their discussion are followed by final conclusions.

2.6.2 3D structural model

For the model geometry, only the hydraulically active fractures with high permeability, as proven by thermal anomalies, detected microseismicity during stimulation and operation (Sausse et al., 2010) and which are intersecting multiple wells were included. The model is thus limited to only 5 major fractures or fault zones as shown in Figure 32.

2.6.3 Meshing of the model

COMSOL Multiphysics version 5.5 (COMSOL) is used to perform numerical modelling of thermo-hydro processes. It uses a finite element method to solve general purpose partial differential equations. The complete mesh contains 53257 domain elements and 2992 boundary elements and 576 edge elements as shown in Figure 33. Total number of degrees of freedom soled are 22622 and additionally internal degrees of freedom are 55848.

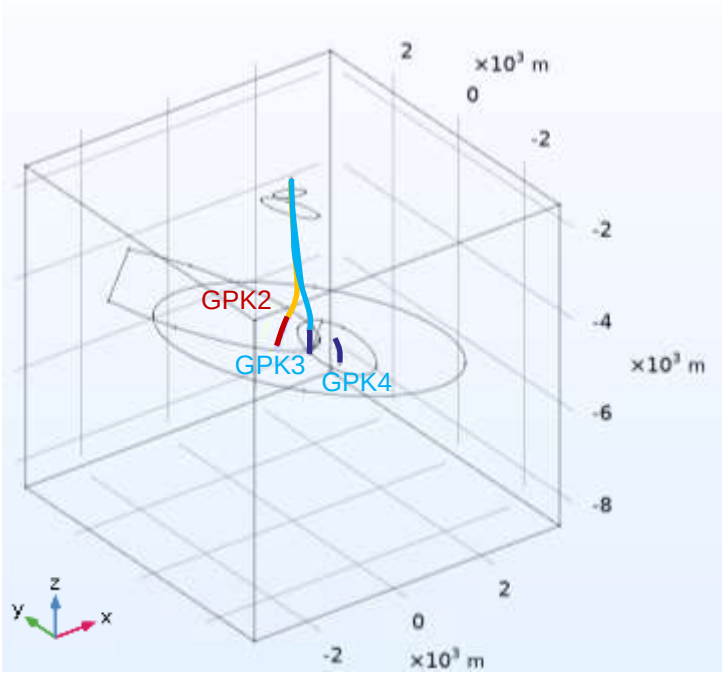

Figure 32: Geometry for numerical modelling of Soultz-sous- Forêts geothermal site.

For the numerical modelling purpose, we have used a scaled absolute tolerance with tolerance factor of 0.1 and automatic time step constraint. We assumed Backward

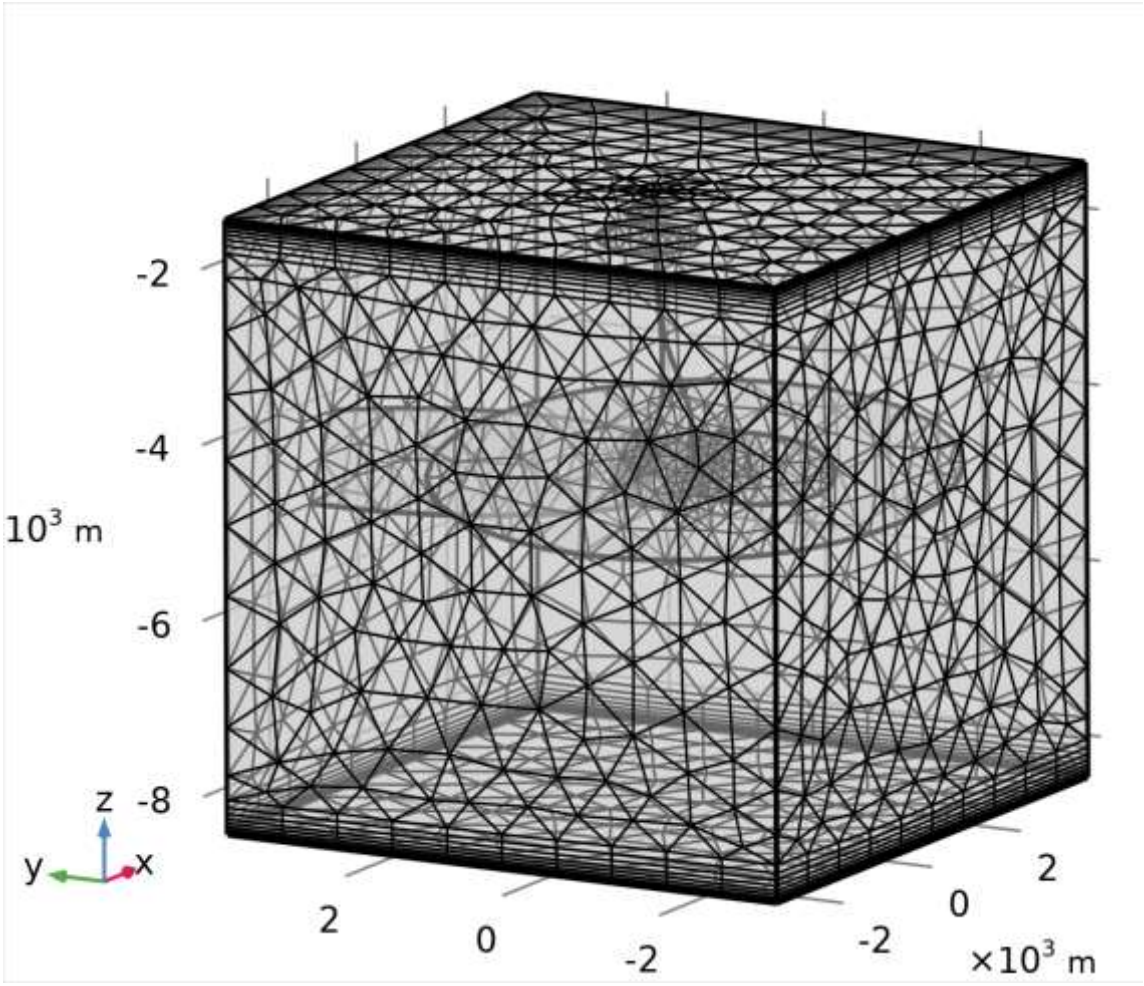

Figure 33: Meshing of the Soultz-sous- Forêts geometry in three dimensional.

Differentiation Formula (BDF) for time stepping with maximum BDF order as 2 and minimum BDF order as 1. Further, we have validated our model with a soil thermal consolidation model as demonstrated by Bai (2005) in Mahmoodpour et al. (2021).

2.6.4 Hydrothermal processes, initial state and boundary conditions

A constant heat flux of 0.07 W/m^2 was assigned at the bottom boundary of the domain. All other exterior boundaries of the modelled domain are defined as no flow for both fluid and heat transmission. Since, the weather conditions of Soultz are not available, the monthly averaged daily weather fluctuation of Strasbourg, France was used for this study. Strasbourg is approximately 40 km SSE from the Soultz geothermal site. All fractures within the domain are regarded as internal boundaries, implicitly considering the mass and energy exchange between porous media and fractures or fault zones. In the injection well, the diameter of the well is small and can as simplification be represented by a line.

The coupled heat and mass transfer in a fractured rock matrix can be modelled using the mass balance equation integrated with heat transport. The governing equation for heat and mass flow in porous media can be written as:

$$\rho_1(\phi_m S_1 + (1-\phi_m)S_m)\frac{\partial p}{\partial t} - \rho_1(\alpha_m(\phi_m\beta_1 + (1-\phi_m)\beta_m))\frac{\partial T}{\partial t} = \nabla.(\frac{\rho_1 k_m}{\mu}\nabla p) \quad [1]$$

In the above equation fluid pressure and temperature in the rock matrix are denoted by p and T respectively. Here rock porosity is ϕ_m, storage coefficients for rock and fluid are S_1 and S_m. The thermal expansion coefficient of the fluid and rock matrix is denoted by β_1 and β_m respectively. The fluid density and dynamic viscosity are indicated using ρ_1 and μ whereas the reservoir permeability is denoted by k_m.

The fractures are assumed as internal boundaries and the flow along the internal fractures can be denoted by:

$$\rho_1(\phi_f S_1 + (1-\phi_f)S_{mf})e_h\frac{\partial p}{\partial t} - \rho_1(\alpha_f(\phi_f\beta_1 + (1-\phi_f)\beta_f))e_h\frac{\partial T}{\partial t} = \nabla_T.\left(\frac{e_h\rho_1 k_f}{\mu}\nabla_T p\right) + n.Q_m \quad [2]$$

Here fluid pressure and temperature in the fracture are indicated by p and T respectively. Additionally, $\phi_f, S_f, \beta_f, e_h$ and k_f denotes the fracture porosity, storage coefficients of the fracture, thermal expansion coefficient of the fracture, hydraulic aperture between the two fracture surfaces, and fracture permeability, respectively. The mass flux exchange between the fracture and matrix are denoted by $n.Q_m = n.(-\frac{\rho k_m}{\mu\nabla p})$ whereas the gradient operator applicable along the fracture tangential plane is indicated by ∇_T.

The local thermal non-equilibrium (LTNE) approach to model heat exchange between the rock matrix and water is implemented in this study. The conductive heat transfer between rock matrix and pore fluid is the dominant heat exchange mechanism. For the rock matrix, the heat transfer equation can be written as

$$(1-\phi_m)\rho_m C_{p,m}\frac{\partial T_m}{\partial t} = \nabla.\left((1-\phi_m)\lambda_m\nabla T_m\right) + q_{ml}(T_l - T_m) \quad [3]$$

In the above equation rock matrix and fluid temperatures are denoted by T_m and T_l, respectively. Here rock density, rock specific heat capacity, rock thermal conductivity and the rock-fluid heat transfer coefficient are denoted by ρ_m, $C_{p,m}$, λ_m and q_{ml} respectively. The heat flux leaving the domain and received by the adjacent fracture can be written as

$$(1-\phi_f)e_h\rho_f C_{p,f}\frac{\partial T_m}{\partial t} = \nabla_T.\left((1-\phi_f)e_h\lambda_f\nabla_T T_m\right) + e_h q_{fl}(T_l - T_m) + n.(-(1-\phi_m)\lambda_m\nabla T_m) \quad [4]$$

where T_m and T_l are the matrix and fluid temperatures in the fracture, respectively; ρ_f is the density of the fracture; $C_{p,f}$ is the specific heat capacity of the fracture; λ_f is the thermal conductivity of the fracture; and q_{fl} represents the rock fracture-fluid interface heat transfer coefficient, related to the fracture aperture. Last term on the right-hand side of the Eq. [4] represents the heat flux exchange between rock matrix and the fracture.

The heat convection equation for the pore fluid can be written as:

$$\phi_m\rho_l C_{p,l}\frac{\partial T_l}{\partial t} + \phi_m\rho_l C_{p,l}(-\frac{k_m\nabla p}{\mu}).\nabla T_l = \nabla.(\phi_m\lambda_l\nabla T_l) + q_{ml}(T_m - T_l) \quad [5]$$

Here $C_{p,l}$ is the heat capacity of the fluid at a constant pressure and λ_l is the thermal conductivity of the fluid.

The heat flux coupling relationship of the fluid between the domain and the fracture is satisfied by:

$$\phi_f e_h\rho_l C_{p,l}\frac{\partial T_l}{\partial t} + \phi_f e_h\rho_l C_{p,l}(-\frac{k_f\nabla_T p}{\mu}).\nabla_T T_l = \nabla_T.\left(\phi_f e_h\lambda_l\nabla_T T_l\right) + e_h q_{fl}(T_m - T_l) + n.q_l \quad [6]$$

where the heat flux $\boldsymbol{n}.\boldsymbol{q_l} = \boldsymbol{n}.(-\boldsymbol{\phi_l}\boldsymbol{\lambda_l}\boldsymbol{\nabla T_l})$ denotes the heat exchange of the fluid between porous media and the fracture.

Temperature-dependent fluid thermodynamic properties are implemented into the coupled hydrothermal mass and energy balance equations. The thermophysical properties of water as a function of temperature including dynamic viscosity ($\boldsymbol{\mu}$), specific heat capacity ($\boldsymbol{C_p}$), density ($\boldsymbol{\rho}$), and thermal diffusivity ($\boldsymbol{\kappa}$) are listed below:

$$\boldsymbol{\mu = 1.38 - 2.12 \times 10^{-2} \times T^1 + 1.36 \times 10^{-4} \times T^2 - 4.65 \times 10^{-7} \times T^3 + 8.90 \times 10^{-10} \times T^4 - 9.08 \times 10^{-13} \times T^5 + 3.85 \times 10^{-16} \times T^6} \quad (\boldsymbol{273.15 - 413.15\ K}) \quad [7]$$

$$\boldsymbol{\mu = 4.01 \times 10^{-3} - 2.11 \times 10^{-5} \times T^1 + 3.86 \times 10^{-8} \times T^2 - 2.40 \times 10^{-11} \times T^3} \quad (\boldsymbol{413.15 - 553.15\ K}) \quad [8]$$

$$\boldsymbol{C_p = 1.20 \times 10^4 - 8.04 \times 10^1 \times T^1 + 3.10 \times 10^{-1} \times T^2 - 5.38 \times 10^{-4} \times T^3 + 3.63 \times 10^{-7} \times T^4} \quad [12]$$

$$\boldsymbol{\rho = 1.03 \times 10^{-5} \times T^3 - 1.34 \times 10^{-2} \times T^2 + 4.97 \times T + 4.32 \times 10^2} \quad [9]$$

$$\boldsymbol{\kappa = -8.69 \times 10^{-1} + 8.95 \times 10^{-3} \times T^1 - 1.58 \times 10^{-5} \times T^2 + 7.98 \times 10^{-9} \times T^3} \quad [10]$$

Understanding the fluid flowing temperature along the wellbore can be useful for an accurate estimation of the overall heat production at the production well head temperature as well as in estimating any possible leakage caused heat loss along the wellbore. Several reliable analytical techniques are reported in literature to calculate the flowing temperature distribution along a wellbore (Alves et al., 1992, Hasan et al. 2009, Moradi et al. 2020).

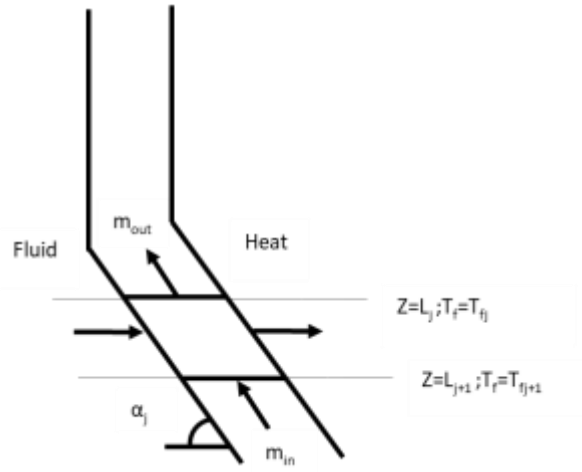

Figure 34: Wellbore heat loss modeling schematic.

We have integrated our reservoir simulation with a wellbore flow model as developed by Hasan et al. (2009). The model constitutes an analytical approach to estimate wellbore-fluid temperature distribution for steady state flow. In this method, the wellbore is split into two uniform sections for thermal properties and deviation angle. The analytical equations are solved sequentially for each section. Figure 34 shows in simplification a typical geothermal well with one deviation angle. The well is inclined at an angle α with the horizontal plane. The heat transfer between wellbore fluid and the rock matrix occurs due

to temperature difference between them. A general energy balance equation for single phase fluid flow can be expressed as:

$$\frac{dH}{dz} - g\,sin\alpha + v\frac{dv}{dz} = \pm\frac{Q}{w} \quad [11]$$

Here, H is the fluid enthalpy, g is gravitational constant, z is the variable well depth from the surface, v is flow velocity, Q is the heat flux per unit of well length and w is the mass rate. When assuming no-phase change conditions, enthalpy will become:

$$dH = (\frac{\partial H}{\partial T})_p dT + (\frac{\partial H}{\partial p})_T dp = c_p dT - C_J c_p dp \quad [12]$$

In the above equation, T is the fluid temperature and p is pressure, c_p is specific heat capacity of fluid, C_J is Joule-Thomson coefficient. If T_f is the fluid temperature, the energy balance equation will be:

$$\frac{dT_f}{dz} = C_J\frac{dp}{dz} + \frac{1}{c_p}(\pm\frac{Q}{W} + g\,sin\alpha - v\frac{dv}{dz}) \quad [13]$$

The heat flux per unit wellbore length can be expressed as:

$$Q \equiv -L_R w c_p (T_f - T_{ei}) \quad [14]$$

Here, T_{ei} is the rock temperature, and L_R is the relaxation parameter defined as:

$$L_R \equiv \frac{2\pi}{c_p w}[\frac{r_{to}U_{to}k_e}{\lambda_m + (r_{to}U_{to}T_D)}] \quad [15]$$

$$T_f = T_{ei} + \frac{1-e^{(z-L)L_R}}{L_R}[g_G\,sin\alpha + \Phi - \frac{g\,sin\alpha}{c_p}] \quad [16]$$

In Eq. (15) and (16), r_{to} is the tubing outside radius, U_{to} is the overall heat transfer coefficient, k_e is rock thermal conductivity, T_D is nondimensional temperature, L is measured depth of wellbore, g_G is the geothermal gradient. and Φ is the lumped parameter and it lumps the kinetic energy term as well as the Joule-Thomson coefficient term.

If V is the fluid specific volume and S is fluid entropy then from Maxwell identities, we can write:

$$(\frac{\partial H}{\partial p})_T = V + T(\frac{\partial S}{\partial p})_T \;\&\; (\frac{\partial S}{\partial p})_T = -(\frac{\partial V}{\partial T})_p \quad [17]$$

$$dH = c_p dT + [V - T(\frac{\partial V}{\partial T})_p]dp \quad [18]$$

$$c_p C_J = -[V - T\left(\frac{\partial V}{\partial T}\right)_p] \quad [19]$$

For liquids if ρ is the liquid density, volume expansivity (β) can be calculated as:

$$\beta \equiv (\frac{1}{V})\left(\frac{\partial V}{\partial T}\right)_p \equiv (-\frac{1}{\rho})(\frac{\partial \rho}{\partial T})_p \quad [20]$$

$$dH = c_p dT + V(1 - \beta T)dp \quad [21]$$

$$c_p C_J = -V(1 - \beta T) \quad [22]$$

Therefore, the final output temperature from the wellhead will be:

$$T_{out} = \frac{\int m\,c_p\,T\,dz}{\int m\,c_p\,dz} \quad [23]$$

In this text, we considered three wells, GPK-3 and GPK-4 as two injection wells and GPK-2 as production wells. In GPK-3, the wellbore leakage was assumed between 1282 m and 4852 m depth measured from the surface. In case of GPK-2, the wellbore leakage was modelled between 1264 m to 4244 m depth measured from the surface. The fluid is single phase water flow and the model parameters are constant specific heat capacity of

water as 4200 J/kg/k, $\boldsymbol{L_R = 0.00001}$ 1/m and $\boldsymbol{\Phi = 0.00345}$ K/m, respectively. Here $\boldsymbol{L_R}$ and $\boldsymbol{\Phi}$ accounts for the casing properties, cement properties and their thicknesses.

2.6.5 Model Calibration

The validation is part of our simulation result and it is discussed in the following section in detail. The overall validation for the proposed methodology in the COMSOL is done in our conceptual studies and it is beyond the scope of the field work.

2.6.6 Simulation and results

In this section, first the hydro-thermal numerical modelling results are compared with the operational data measured at Soultz-sous-Forêts for three years of operation. Furthermore, new injection scenarios are proposed that can be adopted with the existing industrial set-up to enhance the energy extraction capability.

The operational data for three years has been made available for Soultz-sous- Forêts site by the site operators and is used here to calibrate the coupled unsteady hydro-thermal model. Figure 35 shows the injection and production rates at the wellhead for 1163 days from June 2016 to September 2019. The fluid injection temperature is 70°C for both the injection wells.

In Figure 36, the numerical model data is validated with operational data for the time period as described above. The measured temperature data is the operational data for 1163 days at the production wellhead. The temperature at the production well based on the hydro-thermal model is significantly different compared to the operational data. For most of the operational period, the predicted production well temperature is 15°C higher than the measured temperature. Only operation onset and termination stages display smaller deviation in predicted temperature than observed temperature. Since the wellhead temperature measurement may get affected by the local ambient temperature and the monthly average temperature near the geothermal site is almost the same for the corresponding months in each operational year, a correction factor to account for the weather impact on production temperature based on the numerical model was introduced. Two scenarios of seasonal impact are considered, (a) 20% impact of ambient temperature ($T_{effective}=T_{simulation}$ + 0.2×ambient temperature) and (b) 50 % impact of ambient temperature ($T_{effective}=T_{simulation}$ + 0.5×ambient temperature) on the production fluid temperature.

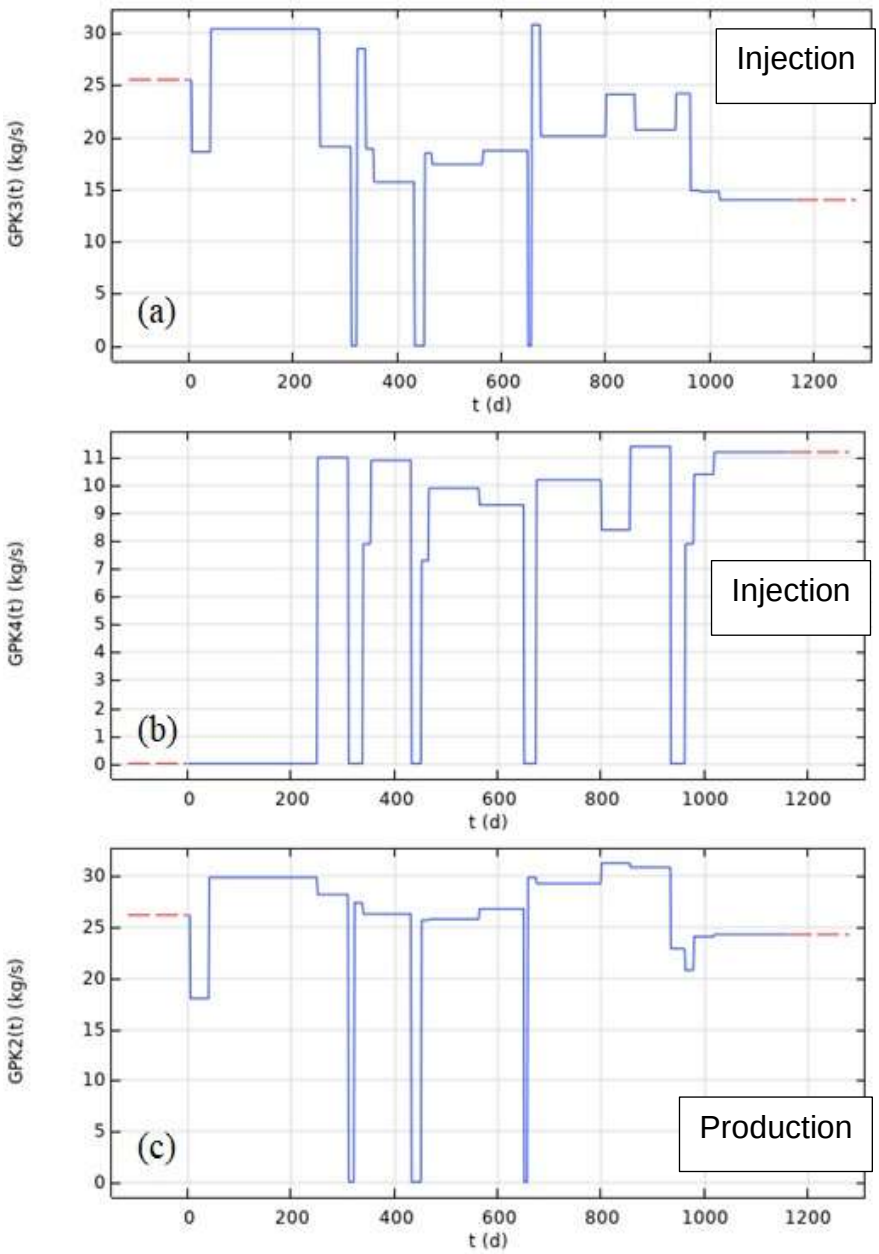

Figure 35: Injection schedule at (a) GPK-3 and (b) GPK-4 and production schedule at production well GPK-2 for 1163 days of operation from June 2016 to September 2019. Here the blue lines are the actual injection and production rates. The red dash lines indicate no operation period.

Figure 36 shows the comparison of the operational data with the coupled reservoir-wellbore model and weather influenced production fluid temperature. The integrated wellbore – reservoir model has the highest overestimation of production temperature. However, when daily weather fluctuation in the integrated wellbore-reservoir model is considered, the prediction matches very well for most part of the operation as shown in Figure 36. The difference between operational and numerical data while considering 50% of the ambient temperature on the production temperature of the coupled wellbore-reservoir model has the best matching among all models. However, the model deviates by more than 15°C from the operation data during the period of 1.8 years and 2.4 years.

Since no other reasons for these deviations are provided with the operational data set, different measurement procedures or false measurements at the wellhead are assumed as reasons for these deviations.

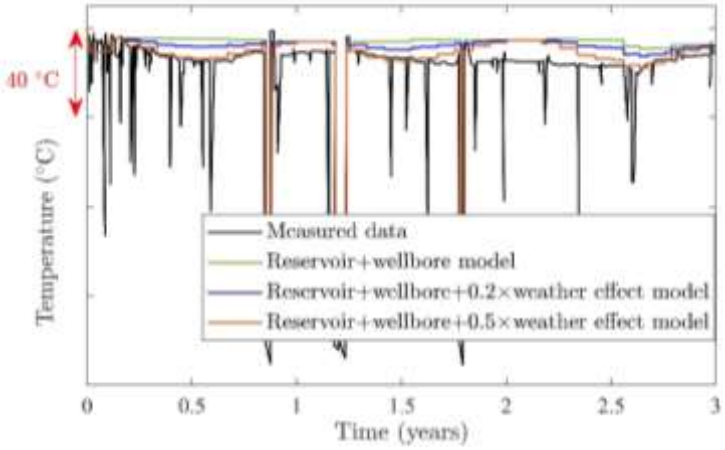

Figure 36: Qualitative difference between operational data from June 2016 to September 2019 and the data obtained from numerical model.

2.7 RESULTS, DISCUSSIONS AND CONCLUSIONS

2.7.1 Cold water reinjection consequences from experiments

In this study, the model was extended to a simulation period of 100 years of operation to predict the wellhead temperature development at the production well. In this section, different initial temperatures at the bottom hole section than the operationally measured data were used. The main objective of this study is to estimate the temperature at the production well (GPK-2) for different injection temperatures for long-term operational periods. Two scenarios were considered, A and B. In both scenarios, the injection rates for the first 1163 days are the same as in the provided operational data set. For the remaining operational period, scenario A considers four different fluid injection temperatures at the injection wellhead (70°C, 60°C, 50°C and 40°C). The fluid injection rates are 13.3 L/s and 11 L/s for GPK-3 and GPK-4, respectively and the production fluid rate from GPK-2 is 24.3 L/s for the remaining operational period. In Scenario B, injection rate post 1163 days are 19.6 L/s and 9.7 L/s for GPK-3 and GPK-4 respectively and the production rate at GPK-2 is 29.3 L/s; the same four injection wellhead temperature as for scenario A were considered, 70°C, 60°C, 50°C and 40°C.

Figure 37 and Figure 39 show the temperature along the wellbore for scenario A and B respectively for both injection wells. The wellbore GPK-3 has an open hole section that causes a linear temperature drop along the wellbore instead of nonlinear temperature drop as shown in Figure 38(a) and Figure 39(a). It is interesting to note that instead of having different injection-production rates in all three wells, the fluid production temperature at GPK-2 wellhead is almost similar for both the scenarios A and B as shown in Figure 37 and Figure 40 respectively. The small increase in temperature at the production wellhead is due to sudden drop in the production wellhead pressure. Also, the temperature increase in scenario B is higher compared to scenario A due to the fact that

scenario B has a higher production rate than scenario A which reduces the time for exchanging heat in the wellbore.

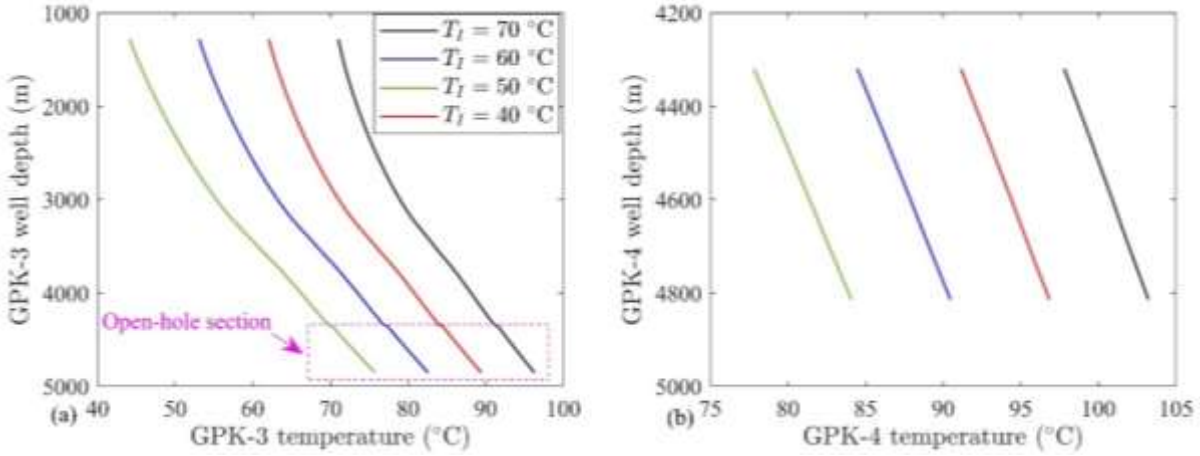

Figure 37: Temperature along the injection wells (a) GPK-3 and (b) GPK-4 with depth for Scenario A.

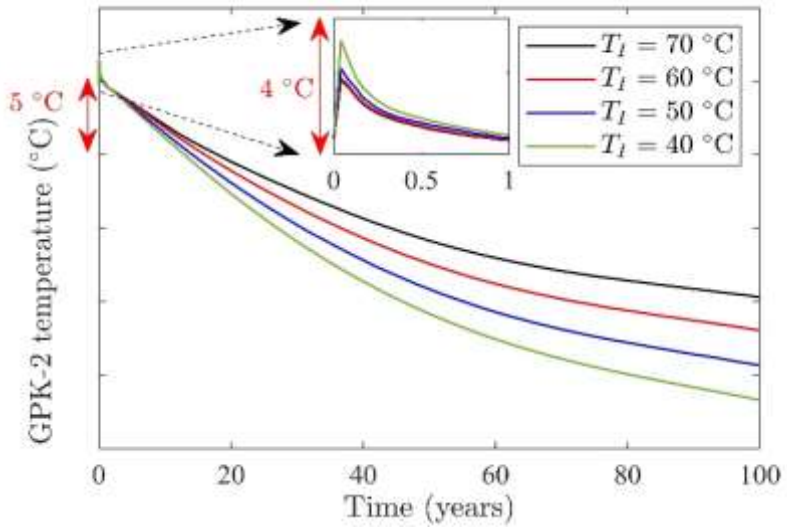

Figure 38: Wellhead temperature at the production well, GPK-2 with time for Scenario A.

Figure 41 shows the comparison of temperature distribution in the fractures and along the wellbore for scenarios A and B. The higher production rate results in slightly faster thermal drawdown at the production well bottom for scenario B than scenario A. No thermal breakthrough was observed at the production well bottom even after 100 years of operation as shown in Figure 41 (e & f).

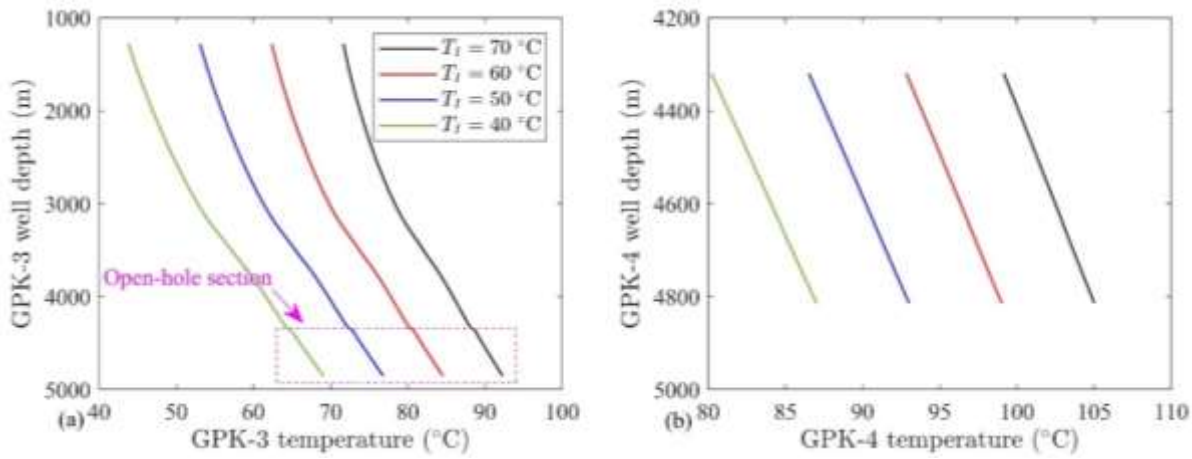

Figure 39: Temperature along the injection wells (a) GPK-3 and (b) GPK-4 with depth for Scenario B.

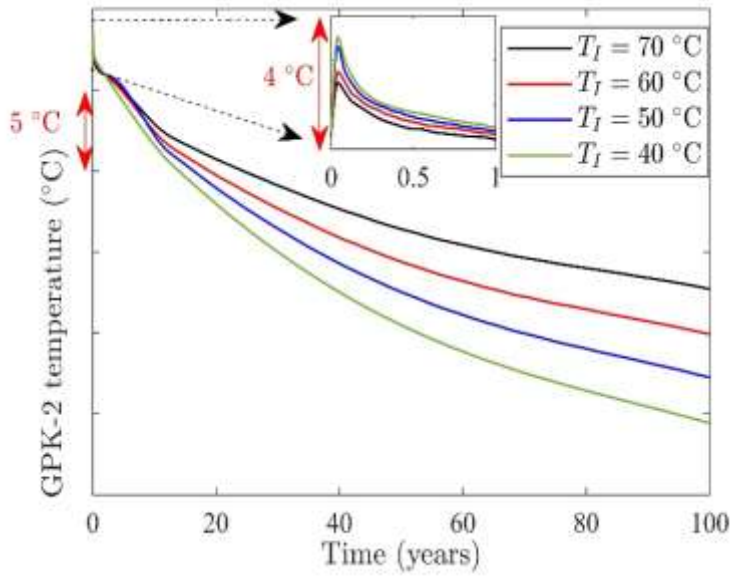

Figure 40: Wellhead temperature at the production well, GPK-2 with time for Scenario B.

A coupled reservoir and wellbore model for hydraulic and thermal processes involved during geothermal energy extraction operation at Soultz-sous-Forêts was developed. Operational data from a period of 1163 days of operation was used to validate the numerical model. The validated hydro-thermal numerical model precisely simulates the geothermal energy extraction operation for 3 years. Furthermore, two operational scenarios for 100 years with four different injection wellhead temperatures 70°C, 60°C, 50°C and 40°C were analysed and it can be observed that even after 100 years of operation, thermal breakthrough at the production well is only in the range of 10 to 20°C. After 100 years of cold fluid injection and hot fluid production, the observed temperature drop at the production wellhead is less than 20°C. Therefore, our numerical model predicts that 100 years of geothermal energy extraction operation at Soultz-sous-Forêts

is feasible and will have sufficiently high production temperature throughout the operation duration.

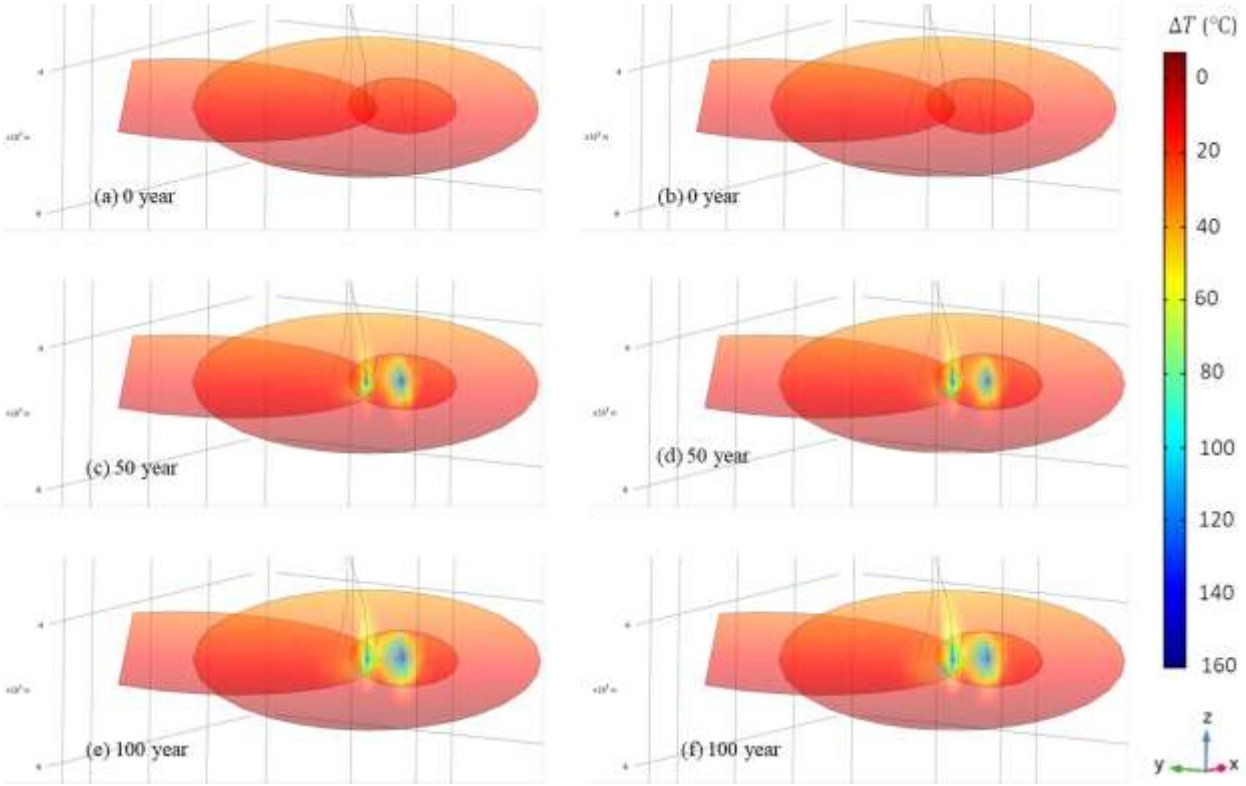

Figure 41: Comparison of temperature distribution (in SI units) in the fractures for scenario A and B. Here ΔT is the temperature drop in the reservoir from the initial state.

As mentioned in section 2.2, the small-scale ORC test realized in Soultz in the framework of MEET did not result in a colder reinjection as the power of this ORC was too small in comparison of the installed main ORC capacity.
Nevertheless, outdoor seasonal variations, leading to injection temperature changes allowed a detailed analysis of the relation of the production temperature with the injection temperature. It shows that a thermal connexion between the production temperature and the injection temperature is developing in the site (5°C decrease of injection temperature leads to 1°C decrease of production temperature).

2.7.2 Outcomes on the conceptual and structural model

The calibration of the first model showed the limitations of the initial structural model behind the simulations. Indeed, it appeared necessary to extend one of the faults to the boundary of the model and to attribute to this structure higher transmissivity values than inferred during the hydraulic tests of the well, in order to get far-field contribution from the reservoir to the system. It is possible that the hydraulic properties of this fault increases with time since testing, as mentioned previously, but this possibly shows that some of the faults included in the model could be connected to great extension structures like the

Soultz horst border faults which have at least 500 m of vertical offset that connect the system to the regional geothermal reservoir.

The necessity to improve the initial geological (and physical) models were also confirmed by VSP analysis as the numerical simulations performed on these models didn't reproduce the important features visible on the real VSP data, mainly the increasing of the seismic signal amplitudes downward, and the triplication of the wave arrivals around - 2200 m depth MSL. Once the structure of the geological model has been improved, the simulations performed from these new models provide better seismic features qualitatively closer to the observed features. These results show us that the improvement of the structural model goes in the right way and could be close to the real geology. A blocky basement (at least at the top) with different physical parameters values for each block seems to be the correct way to explain the data.

This observation is confirmed by the results of the model.

The final structural model built from 3D seismic interpretation data, VSP data and well logging data is representative of the reservoir as it could reproduce the flow distribution at the wells, the wellhead pressures and the production temperature evolution with time on the calibration period used for history matching.

2.7.3 Considerations on the methodological approaches

Interestingly, the simulations presented in this report were carried out using 3 different numerical codes:

- The first model was run using the commercial code FEFLOW, using MeshIt for meshing purpose.
- The second model was run using the commercial code Eclipse, using Petrel for gridding and Re-Studio for pre-processing.
- The third model was run using COMSOL Multiphysics.

The workflow and results comparisons allow to draw conclusion regarding the application of these codes to geothermal models in fractured rocks. These conclusions can be summarized as:

- The use of FEFLOW is adapted to industrial use, offering fast computation time. Highly conductive discrete structures could be simulated smoothly. Nevertheless, FEFLOW application is limited to hydrothermal (and transport) simulations, and the meshing step requires fine tuning and is very time consuming.
- Eclipse allows fast gridding through PETREL and fast computation, but the integration of highly conductive discrete features is a challenge.
- COMSOL Multiphysics allows to take in account multiple physical processes, as mechanical or poro-elastic processes, but calculations are time intensive.

2.7.4 Colder reinjections consequences on the reservoir

The simulation results show that:

- **A temporary decrease (over a few months) of the injection temperature does not affect the production temperature over a long time**, as the production temperature comes back to the initial production temperature after maximum 2 years.
- **A long-term decrease in the injection temperature will have a limited effect on the production temperature.** According to the models, a 10 °C injection temperature decrease in GPK-3 and GPK-4 is expected to produce a drop of up to 3 °C on production temperature at GPK-2 over 30 years.
- **Moreover, a colder reinjection does not significantly affect the temperature distribution in the reservoir**. The cold front does not propagate faster, and the "cooled-down" volume reaches a lower temperature at its core but the temperature impact at the fringe remains limited, because as the cold fluid will finally drain more energy from the surrounding rock. This is the reason why the temperature impact at the production well remains limited.
- The colder reinjection has very limited impact on thermal breakthrough even after 100 years of operation. The wellbore effect is significantly important production temperature.

To summarize, a significant decrease of injection temperature (from 70°C down to 40°C) in order to produce more energy appears to have a clear but limited impact on the reservoir and on the production temperature. This impact is mainly due to fast connections, likely to occur in the upper part of the reservoir, due to production casing integrity issues.

Thus, from a reservoir point of view, this work confirms that using colder injections to increase the total produced energy is perfectly feasible.

2.8 REFERENCES

Agemar T., Schellschmidt R., Schulz R., 2012. Subsurface temperature distribution in Germany. Geothermics 44, 65-77. https://doi.org/10.1016/j.geothermics.2012.07.002

Aichholzer C., Duringer P., Orciani S., Genter A., 2016. New stratigraphic interpretation of the Soultz-sous-Forêts 30-year-old geothermal wells calibrated on the recent one from Rittershoffen (Upper Rhine Graben, France). Geotherm. Energy 4 (1), 13. https://doi.org/10.1186/s40517-016-0055-7.

Alves, I.N.; Alhanatl, F.J.S.; Shoham, O. A unified model for predicting flowing temperature distribution in wellbores and pipelines. SPE Prod. Eng, November 1992, 363-367.

Bai, B., "One-dimensional thermal consolidation characteristics of geotechnical media under non-isothermal condition", Eng. Mech., 22, p: 186-191, 2005.

Baillieux O., Schill E., Edel J.-B., Mauri G., 2013. Localization of temperature anomalies in the Upper Rhine Graben: insights from geophysics and neotectonics activity. Int. Geol. Rev. 55, 1744-1762.

Baujard, C., Rolin, P., Dalmais, E., Hehn, R. and Genter, A., 2021. Soultz-sous-Forêts geothermal reservoir: structural model up-date and thermo-hydraulic numerical simulations based on 3 years operation data, submitted to Geosciences

Blumenthal M., Kühn M., Pape H., Rath V., Clauser C., 2007. Hydraulic model of the deep reservoir quantifying the multi-well tracer test. Presented in Proceedings of the EHDRA Scientific Conference, 28-29 June 2007, Soultz-sous-Forêts, France.

Cacace, M., Blöcher, G., 2015. MeshIt - a software for three dimensional volumetric meshing of complex faulted reservoirs. Environ. Earth. Sci., 74, 5191–5209, https://doi.org/10.1007/s12665-015-4537-x

COMSOL Multiphysics® v. 5.5. www.comsol.com. COMSOL AB, Stockholm, Sweden.

Evans K., Genter A., Sausse J., 2005. Permeability creation and damage due to fluid injections into granite at 3.5 km at Soultz: 1. Borehole observations. Journal of geophysical research 110, B04203, https://doi.org/10.1029/2004JB003168.

Gessner K., Kühn M., Rath V., Kosack C., Blumenthal M., Clauser C., 2009. Coupled process models as a tool for analysing hydrothermal systems. Surv. Geophys. 30(3), 133-162. https://doi.org/10.1007/s10712-009-9067-1.

Hasan, A.R.; Kabir, C.S.; Wang, X. A robust steady-state model for flowing fluid temperature in complex wells. SPE Prod. Operat., May 2009, 269-276.

Dezayes C., Genter A., Chèvremont P., Homeier G., Hooijkaas G., Tourlière B., Stein G., Degouy M., 2005. Deep seated geology of the Soultz basement based on geological data of GPK3 and GPK4 wells. EHDRA Scientific Meeting.

Dezayes C., Courrioux G., Calcagno P., Tourlière B., Chèvremont P., Sausse J., Place J., 2010. Des données géologiques aux modèles 3D du site EGS de Soultz-sous-Forêts (Alsace, France) (No. RP-57927-FR). BRGM, Orléans, France.

Dezayes, C., Genter, A., Valley, B., 2010. Structure of the low permeable naturally fractured geothermal reservoir at Soultz. C. R. Geoscience 342, 517–530. https://doi.org/10.1016/j.crte.2009.10.002

Egert R., Gholami Korzani M., Held S., Kohl T., 2019. Implications on large-scale flow of the fractured EGS reservoir Soultz inferred from hydraulic data and tracer experiments. Geothermics 84. https://doi.org/10.1016/j.geothermics.2019.101749

Gentier S., Rachez X., Tien Dung Tran Ngoc, Peter-Borie M., Souque C., 2010. 3D Flow modelling of the medium-term circulation test performed in the deep geothermal site of Soultz-sous-Forêts (France). World Geothermal Congress 2010.

Gerard A., Genter A., Kohl T., Lutz P., Rose P., Rummel F., 2006. The deep EGS (Enhanced Geothermal System) project at Soultz-sous-Forêts (Alsace, France). Geothermics 35, 502-516.

Held S., Genter A., Kohl T., Kölbel T., Sausse J., Schoenball M., 2014. Economic evaluation of geothermal reservoir performance through modelling the complexity of the operating EGS in

Soultz-sous-Forêts. Geothermics 41, 270-280. http://dx.doi.org/10.1016/j.geothermics.2014.01.016.

Jung R., Willis-Richard J., Nicholls J., Bertozzi A., Heinemann B. 1995. Evaluation of hydraulic tests at Soultz-sous-Forêts, European HDR site. World Geothermal Congress, 2611-2616.

Mahmoodpour, S., Singh, M., Turan, A., Bär, K., Sass, I., "Key parameters affecting the performance of fractured geothermal reservoirs: a sensitivity analysis by thermo-hydraulic-mechanical simulation", http://arxiv.org/abs/2107.02277.

Megel, T., Kohl, T., Gérard, A., Rybach, L., Hopkirk, R., 2005, Downhole Pressures Derived from Wellhead Measurements during Hydraulic Experiments, World Geothermal Congress 2005, 2005, Antalya, Turkey.

Menjoz A., Cautru J.P., Criaud A., Genter A., 1988. Stimulation des réservoirs géothermiques en milieu cristallin – Caractérisation des réservoirs fracturés. Rapport annuel d'activités 1988. BRGM/IMRG Orléans, France, 35-39.

Moradi, B.; Ayoub, M.; Bataee, M.; Mohammadian, E. Calculation of temperature profile in injection wells. J. Pet. Explor. Prod. Tec., 2020, 10, 687-697.

Musa A., Hua-Peng Chen, 2017. Sensitivity analysis of deep geothermal reservoir: effect of reservoir parameters on production temperature. Energy 129, 101-113. http://dx.doi.org/10.1016/j.energy.2017.04.091.

Nami P., Pfender M., Tischner T., 2006. Test series in March 2006 to identify and quantify outlet zones in the three wells GPK2, GPK3 and GPK4. Field Report. BGR.

Place J., 2010. Caractérisation des chemins de circulations de fluides dans le réseau poreux d'un batholite granitique, application au site géothermique de Soultz-sous-Forêt. (PhD). Université de Strasbourg, France.

Pribnow D., Schellschmidt R., 2000. Thermal tracking of upper crustal fluid flow in the Rhine Graben. Geophys. Res. Lett. 27 (13), 1957-1960.

Renard P., Courrioux G., 1994. Three-dimensional geometric modelling of a faulted domain: the Soultz horst example (Alsace, France). Computers & Geosciences vol. 20 no 9, 1379-1390.

Richard, A., Maurer, V., Toubiana, H., Carriere, X., Genter, A., 2020+1. How to Upscale Geothermal Energy from Deep Fractured Basement in the Upper Rhine Graben? The Impact of a New 3D Seismic Dataset, World Geothermal Congress 2021, October 24 - 27 2021, Reykjavik, Iceland.

Sausse J., Dezayes C., Dorbath L., Genter A., Place J., 2010. 3D model of fracture zones at Soultz-sous-Forêts based on geological data, image logs, induced microseismicity and vertical seismic profiles. C. R. Geoscience 342, 531-545, https://doi.org/10.1016/j.crte.2010.01.011.

Sanjuan B., Pinault J.-L., Rose P., Gérard A., Brach M., Braibant G., Crouzet C., Foucher J.-C., Gautier A., Touzelet S., 2006. Tracer testing of the geothermal heat exchanger at Soultz-sous-

Forêts (France) between 2000 and 2005. Geothermics 35 (2006), 622-653. https://doi.org/10.1016/j.geothermics.2006.09.007

Schindler M., Nami P., 2008, “Chronology of casing leaks in GPK4”, unpublished report, EEIG Heat Mining, Rote de Soultz, F-67250 Kutzenhausen, France.

Imprint

Project Lead	ES-Géothermie 26 boulevard du Président Wilson 67932 Strasbourg Cedex 9, FRANCE https://geothermie.es.fr/en/	
Project Coordinator	Dr Albert Genter albert.genter@es.fr	Eléonore Dalmais eleonore.dalmais@es.fr
Scientific Manager	Dr Ghislain Trullenque Ghislain.TRULLENQUE@unilasalle.fr	
Project Manager	Dr Jean Herisson jherisson@ayming.com	
Project Website	https://www.meet-h2020.com/	
LinkedIn page	https://www.linkedin.com/in/meet-eu-project/	
Report Authorship	BAUJARD C., DALMAIS E., ABDELFETTAH Y., BARNES C., SINGH M., MAHMOODPOUR S., (2021). Hydro-thermal model using VSP analysis and colder reinjection tests, MEET report, Deliverable D3.10, September 2021, 57 pp.	

Liability claim